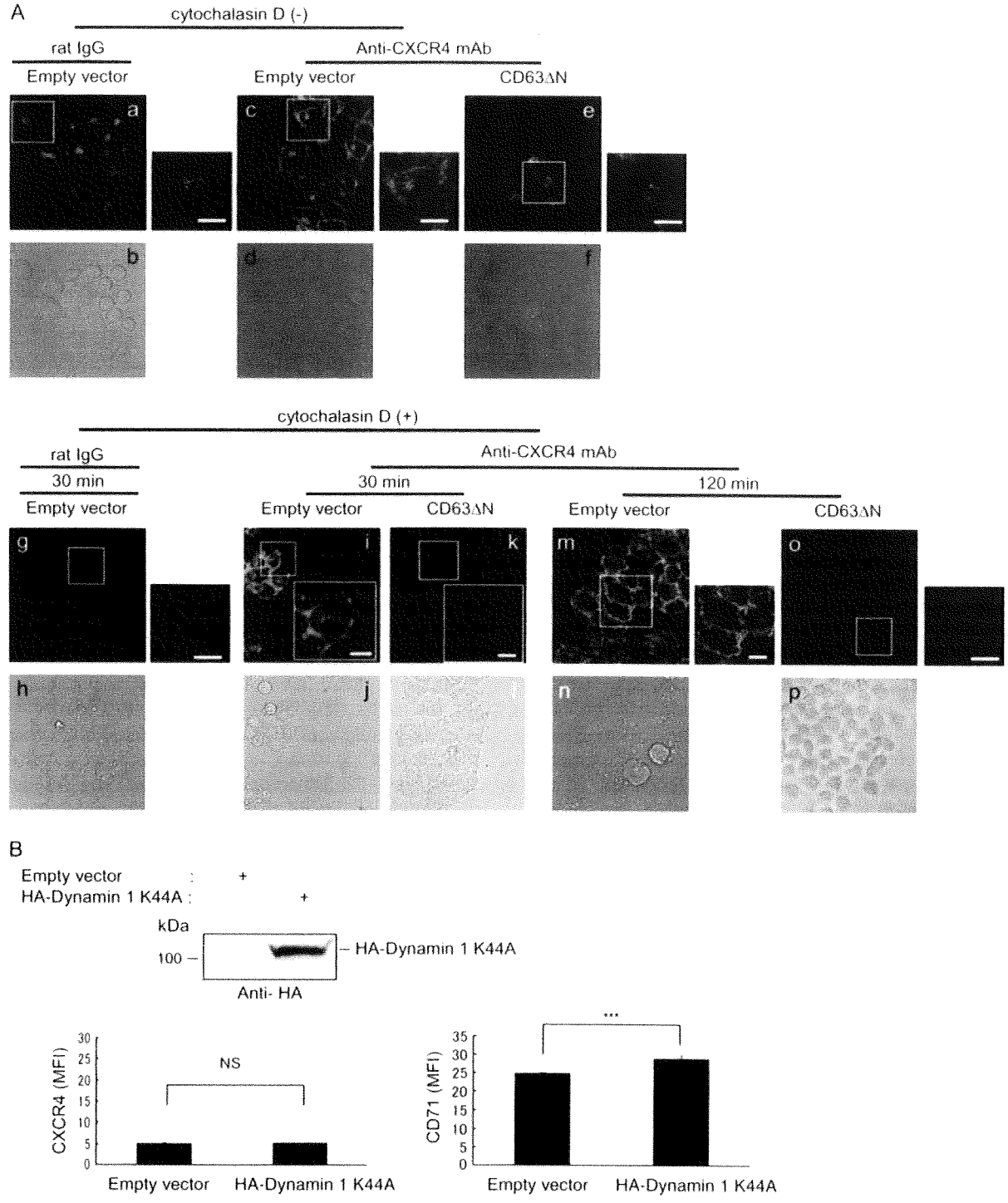


**Figure 5: Absence of CXCR4 from cell surface might not be because of dynamin-dependent internalization.** A) No detectable CXCR4 surface expression on CD63ΔN-transduced MAGIC-5 cells. Empty vector- and CD63ΔN-transduced cells were cultured in the presence of an FITC-labeled anti-CXCR4 mAb (A-145) for 30 min (a–f) and then analyzed by confocal microscopy. Cells supplemented with cytochalasin D (5 μM) were also cultured for 30 min (g–l) or 120 min (m–p). Enlarged images are shown in white boxes. Images were acquired through BPF 500–520 nm (CXCR4: green). Scale bars, 10 μm. DIC images are also shown (lower panel). B) CD71 but not CXCR4 surface expression was increased by dominant negative mutant of dynamin 1-transfection. CD63ΔN-transduced MAGIC-5 cells were transfected with HA-tagged Dynamin 1 K44A DNA. The expression of HA-tagged protein was confirmed by Western blotting (upper panel), and CXCR4 (lower left panel) or CD71 (lower right panel) surface expression was measured by flow cytometry. MFI of CXCR4 or CD71 was shown. Data are represented as mean ± SED, $n = 4$, $^{***}P < 0.05$, NS, not significant.

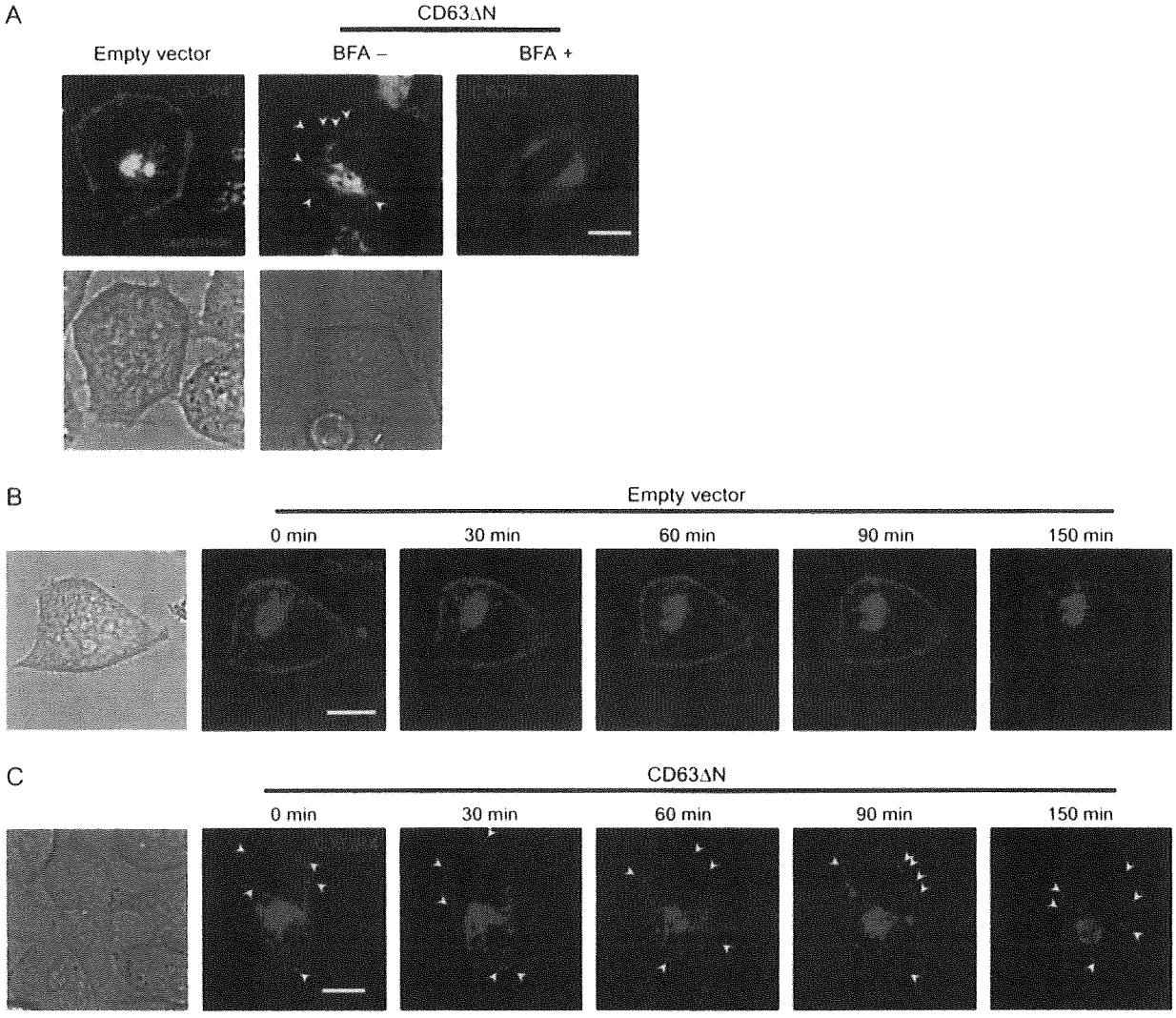


**Figure 6: Intracellular trafficking of CXCR4 via transport vesicles is not inhibited.** A) Localization of CXCR4 in live cells. MAGIC-5 cells were transfected with pHalo-CXCR4, stained with the Halo-ligand and ceramide (Golgi apparatus) and analyzed by confocal microscopy. Right panel shows cells cultured in medium containing 50 μg/mL of BFA without ceramide-staining. Images were acquired through band-pass filters (BPF) 500–520 nm (ceramide: green) and BPF 570–610 nm (CXCR4: magenta). Arrow heads indicate CXCR4-containing vesicles. Scale bars, 10 μm. DIC images are also shown (lower panel). B, C) Longitudinal analyses on the distribution of CXCR4. Cells were followed with confocal microscopy at the indicated time after initiation of the trace. Empty vector-transduced (B) and CD63ΔN-transduced (C) MAGIC-5 cells were studied. Arrow heads in (C) indicate CXCR4-containing vesicles in CD63ΔN-transduced cells. Scale bars, 10 μm. DIC images are also shown (first panels in B, C). D, E) empty vector-transduced (D) or CD63ΔN- transduced (E) MAGIC-5 cells were transfected with CXCR4EGFP and analyzed using TIRFM. DIC images are shown (upper right panels in D and E). Enlarged images from upper left panels in D and E (box) taken at 1-second interval are shown in middle and lower panels. Fusion-like processes between the vesicle and the plasma membrane was detected in empty vector-transduced but not in CD63ΔN-transduced cells. Arrows in middle panels in (E) indicate fusion-like process between a vesicle and the plasma membrane. Images were acquired through BPF 509–547 nm (GFP). Dotted lines indicate the plasma membrane. Scale bars, 10 μm (upper panel) and 1.7 μm (lower panel). sec, second. Figure 6 continued on next page.

number of the vesicles in both empty vector- and CD63ΔN-transduced cells (Table 1). These data suggest that the CD63ΔN-induced CXCR4 mislocalization is not because of inhibition of CXCR4 trafficking via transport vesicles. CXCR4 is suggested to be transported to intracellular organelles, but not to the plasma membrane. As precise quantification of fusion to the plasma membrane was difficult in this assay, we were not able to quantify the fusion events. Interestingly, however, we could capture some fusion-like processes between CXCR4-containing vesicles and the plasma membrane in empty vector-transduced cells (one of them was shown in Figure 6D, arrows in middle panels) but not in CD63ΔN-transduced cells (Figure 6E).

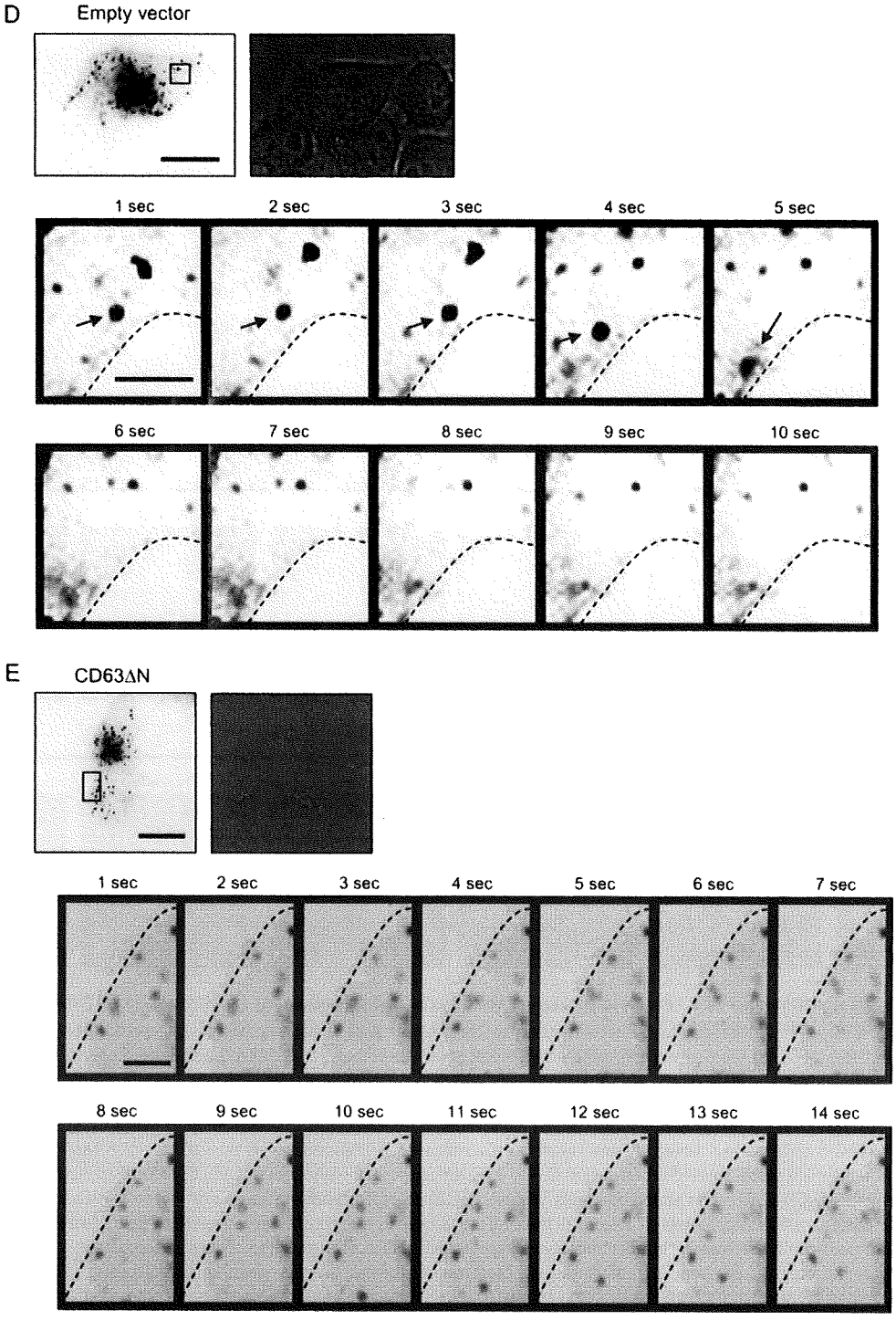


**Figure 6: Continued from previous page.**

### *Mislocalized CXCR4 appears to be destined in the late endosomes/lysosomes*

To investigate the mislocalization of CXCR4 further, we carried out a series of immunofluorescent staining using antibodies against marker molecules in several different organelles. Figure 7A shows that the intracellular CXCR4 in CD63ΔN-transduced cells were predominantly located in the *cis*-Golgi (Golgi matrix protein of 130 kDa: GM130), the TGN (p230) and the late endosomes/lysosomes (LAMP-1), but not in the early endosomes (early endosome antigen 1,

**Table 1:** Quantification of CXCR4-containing vesicles[a]

| | Counted cells | Total | Average (per a cell[b]) |
|---|---|---|---|
| Empty vector | 9 | 1144 | 127.1 |
| CD63ΔN | 19 | 2257 | 118.8 |

[a]Number of vesicles was counted by BASIC METAMORPH software.
[b]Number of vesicles was divided by numbers of cells.

EEA1). It was also partly located in the ER (calnexin) and the vesicles and tubular clusters (ERGIC-53). We also found that a large fraction of intracellular CXCR4 co-localized with lysosome marker, a low internal pH indicator; LysoTracker in CD63ΔN-transduced MAGIC-5 cells transfected with phrGFPCXCR4 (Figure 7A, right panels). The ratio of the merged area where CXCR4 localized with each intracellular organelle is shown in Figure 7B. This graph shows that no CXCR4 is retained in any specific organelle and that the CXCR4 appears to be transported to the late endosomes/lysosomes. By contrast, in empty vector-transduced cells, CXCR4 was mainly found at the plasma membrane and additionally in the ER (Figure S2). We next assessed whether or not CXCR4 is destined to the lysosome-dependent degradation in CD63ΔN-transduced cells using lysosomal inhibitors (chloroquine, CHQ or concanamycin A, CMA) (Figure 7C). In the inhibitor-treated cells, CXCR4 degradation after CHX treatment was clearly inhibited, indicating that most CXCR4 was transported to lysosomes and subsequently degraded in CD63ΔN-transduced cells.

### *CD63ΔN co-localizes and interacts with CXCR4*

To investigate the intracellular co-localization of CD63ΔN and CXCR4, we prepared a FLAG-tagged CD63ΔN (FLAGCD63ΔN)-expressing lentiviral vector and confirmed that its ability to suppress CXCR4 surface expression was similar to that of untagged vector (data not shown). Then, we examined the co-localization of CD63ΔN and CXCR4 in FLAGCD63ΔN-transduced MAGIC-5 cells using confocal microscopy. As shown in Figure 8A, CD63ΔN molecules mainly overlapped with CXCR4 in the perinuclear region. Similar co-localization of CD63ΔN and CXCR4 was also reproduced in 293T cells co-transfected with phrGFPCXCR4 and a red fluorescent protein–tagged CD63ΔN DNA (DsRed-CD63ΔN) (data not shown). Further immunofluorescent staining experiments using antibodies against organelles marker molecules indicated that CD63ΔN was mainly localized in the late endosomes and the TGN (Figure 8B). To gain insight into the relationship between CD63ΔN and CXCR4, we next examined intracellular interaction between these molecules. In addition to CD63ΔN, CD63wt was also examined. As shown in right panel of Figure 8C, CD63ΔN and CD63wt co-precipitated with CXCR4 in 293T cells co-transfected with hemagglutinin (HA)-tagged CXCR4 DNA (pHA-CXCR4) and a FLAG-tagged CD63ΔN or CD63wt DNA. The affinity of CD63ΔN to CXCR4 appeared to be higher than that of CD63wt. CD63wt but not CD63ΔN had an ability to interact with MT1-MMP as reported previously (20).

### *Requirement of a CXCR4 C-terminal cytoplasmic tail for CD63ΔN-induced suppression in CXCR4 surface expression*

To explore the responsible region of CXCR4 for the CD63ΔN-induced suppression, we used a series of EGFP-tagged CXCR4 C-terminal cytoplasmic tail-deletion mutant DNA (C-terminal tail; 14 amino acids from C-termini) (26) (Figure 9A) and transfected them into empty vector- or CD63ΔN-transduced MAGIC-5 cells. Having confirmed that these mutants were expressed on the cell surface of empty vector-transduced cells (data not shown), we measured CXCR4 mutant surface expression on CD63ΔN-transduced cells using flow cytometry. Interestingly, we found that CXCR4 surface expression was sustained in cells transfected with a mutant lacking six amino acids in the C-terminal tail (Figure 9B). The distribution of CXCR4EGFP or these mutants in CD63ΔN-transduced MAGIC-5 cells is also shown in Figure 9C. These mutants but not CXCR4EGFP (wild type) were localized at the plasma membrane. From these data, we deduced that this six amino acid-deletion provided resistance to the CD63ΔN-induced suppression of CXCR4 surface expression. We observed a similar phenomenon in 293T cells co-transfected with CD63ΔN and EGFP-tagged CXCR4-deletion mutant DNA (data not shown). These results indicate that the C-terminal six amino acids ($^{347}$SSFHSS$^{352}$) are involved in the CD63ΔN-induced suppression of CXCR4.

## Discussion

In this study, we successfully identified a mutant of a tetraspanin protein (CD63ΔN) as an inhibitor of X4 HIV-1-induced CPE by our screening strategy using a novel cDNA library-expressing lentiviral vector system (2). Then, we showed that CD63ΔN inhibited X4 HIV-1 infection (Figure 1E,G). The inhibition was observed in X4 HIV-1 but not in MLV-pseudotyped HIV-1 (Figure 1F) or R5 HIV-1 (Figure 1G). Because the difference between X4 HIV-1 and R5 HIV-1 lies upon co-receptor usage at the viral entry, we predicted and confirmed that CD63ΔN induced the suppression of CXCR4 surface expression (Figure 2A,D). These data provide the evidence that localization of co-receptor molecules at the plasma membrane is crucial for HIV-1 entry and by depleting the surface expression of co-receptor proteins, HIV-1 target cells can effectively escape from its infection.

It has been shown that anti-CD63 Ab (27) or recombinant soluble CD63-EC2 proteins (28) inhibited HIV infection in macrophages without affecting expression of CD4 or co-receptor. However, we clearly showed that a CD63 N-terminal deletion mutant blocks X4 HIV-1 entry via specific suppression of CXCR4 surface expression on target cells (Figure 2A,D,E–G). It has not been yet reported that CD63 or its mutants induce downregulation of CXCR4.

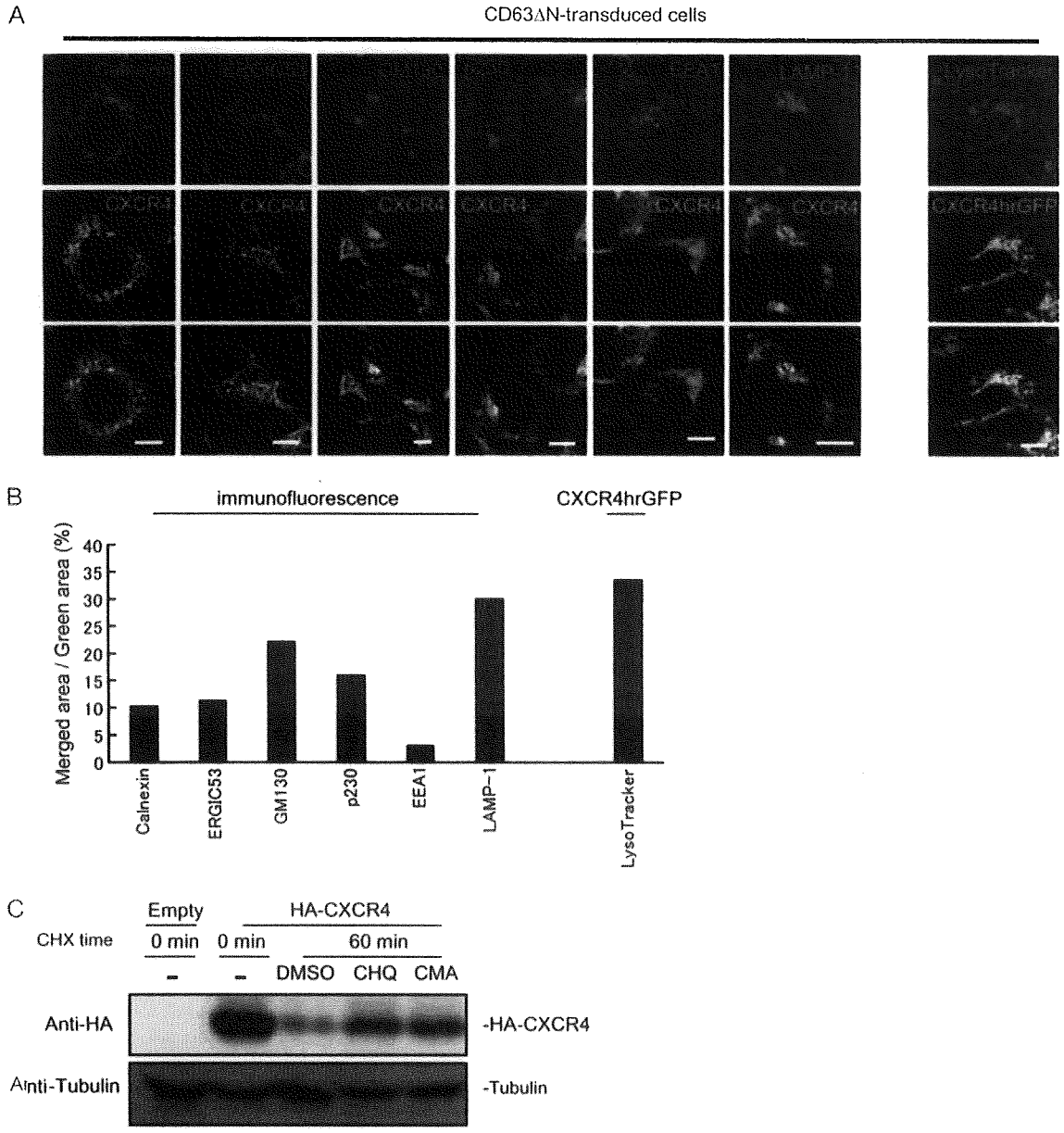


**Figure 7: CXCR4 was transported only toward intracellular organelles.** A) Co-localization of CXCR4 with intracellular organelles in CD63ΔN-transduced MAGIC-5 cells. Images were acquired through band-pass filters (BPF) 500–520 nm (CXCR4 and CXCR4hrGFP: green), BPF 650–700 nm (intracellular organelles: magenta) and BPF 420–450 nm (LysoTracker: magenta). Merged images are shown in bottom. Scale bars, 10 μm. Calnexin: ER; ERGIC53: Vesicular-tubular transport complex (VTCs); GM130: *cis*-Golgi; p230: TGN; EEA1: early endosomes; and LAMP-1: late endosomes. B) The ratio of merged area where CXCR4 co-localized with each intracellular organelle in (A) (merged area/CXCR4 area) was shown. C) The lysosome-dependent degradation of HA-tagged CXCR4 in CD63ΔN-transduced MAGIC-5 cells. The degradation of CXCR4 in the presence of CHX with two classes of lysosomal inhibitors, CHQ (50 μg/mL), CMA (20 μg/mL) or vehicle (DMSO), was assessed by Western blotting. Tubulin served as a control. The results of one of three, independently conducted, experiments are shown.

Although these previous findings and our presented phenomena seem to occur by distinct mechanisms, it might be true that CD63 has some functions in HIV infection.

By flow cytometric analyses, we confirmed the CD63ΔN-induced CXCR4 downregulation in MT-4 (Figure 2A), MAGIC-5 (Figure 2D) and 293T cells (data not shown) as well as human primary $CD4^+$ T cells (Figure 2F), natural target cells for HIV-1. These data suggest that this CD63ΔN-induced suppression is not a cell type-dependent phenomenon. The significant but lower suppression of CXCR4 in $CD4^+$ T cells (Figure 2F) can be explained by the lower efficiency of lentiviral transduction. Also, primary $CD4^+$ T cells needed to be activated with immobilized

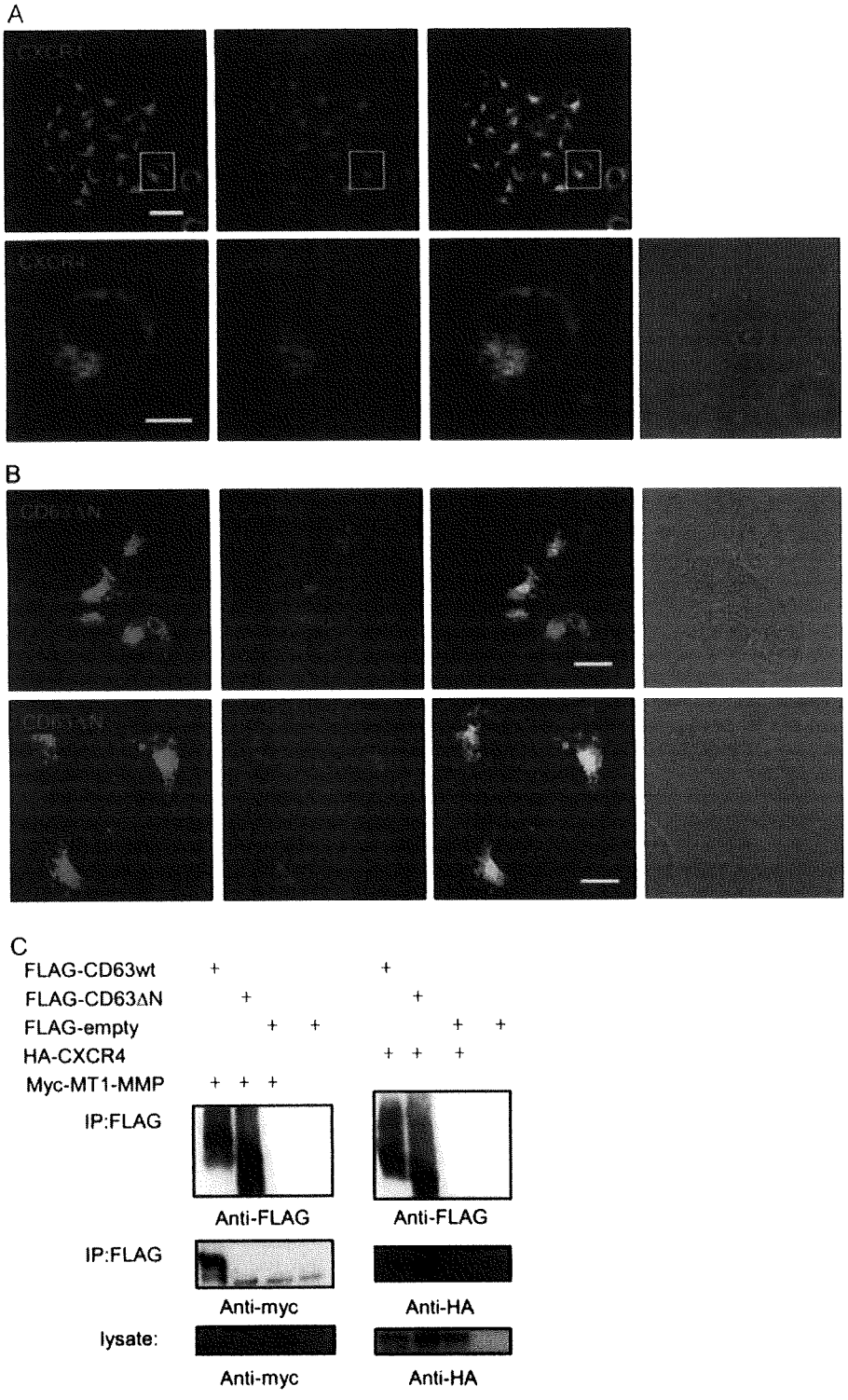


**Figure 8: Co-distribution and interaction of CD63ΔN with CXCR4.** A) Localization of CXCR4 and CD63ΔN. FLAGCD63ΔN-transduced MAGIC-5 cells were stained with an anti-CXCR4 mAb and an anti-FLAG pAb. Images were acquired through band-pass filters (BPF) 500–520 nm (CXCR4: green) and BPF 650–700 nm (FLAG: magenta) and merged images are shown. Scale bars, 50 μm (upper panels) and 10 μm (lower panels). B) Co-localization of FLAGCD63ΔN with intracellular organelles in FLAGCD63ΔN-transduced MAGIC-5 cells. Images were acquired through BPF 500–520 nm (FLAG: green) and BPF 650–700 nm (intracellular organelles: magenta). Merged images are shown in third panels. Scale bars, 10 μm. LAMP-1, late endosomes; and p230: TGN. C) Molecular interaction between CXCR4 and CD63ΔN or CD63wt. FLAG-tagged CD63ΔN or CD63wt were immunoprecipitated (IP) with an anti-FLAG mAbs and immunoblotted with an anti-HA and an anti-FLAG mAb (right panel). Lysate were also subjected to Western blot to detect expression of HA-tagged CXCR4. Interaction between CD63wt and MT1-MMP was shown as a control (left panel). The results of one of three, independently conducted, experiments are shown.

anti-CD3/CD28 mAbs during lentiviral transduction. As CXCR4 surface expression is reduced on activated $CD4^+$ T cells (29), primary $CD4^+$ T cells had lower expression of CXCR4 compared with that of cell lines to start with. In addition to flow cytometric analyses, we confirmed the CXCR4 downregulation by immunofluorescent analysis without permeabilization (Figure 2E) and the reduced response to SDF-1 by CD63ΔN-transduced cells (Figure 2G).

CD63 is known to form TEMs on the plasma membrane with other tetraspanin proteins (11). Do TEMs play any role

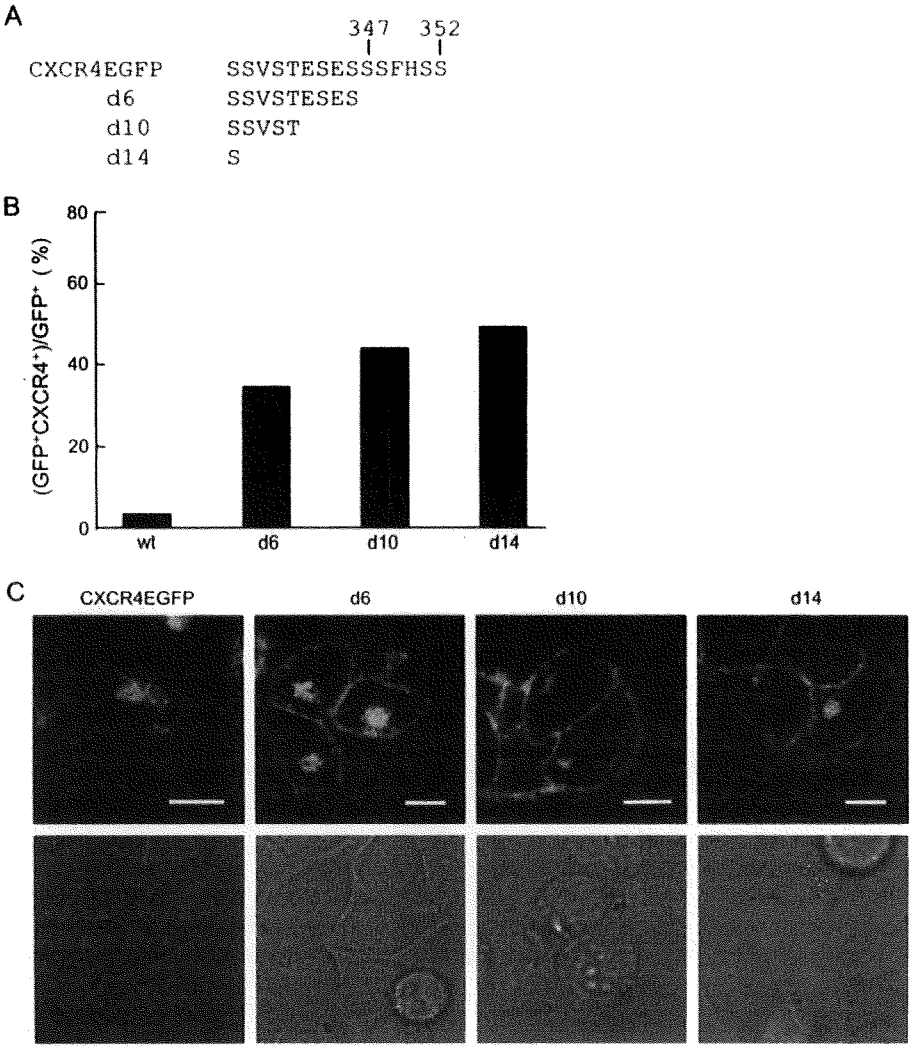


**Figure 9: Requirement of CXCR4 C-terminal cytoplasmic tail for CD63ΔN-induced suppression in CXCR4 surface expression.** A) Amino acid sequence of the C-terminal tail of CXCR4. Shown is the amino acid sequence (single-letter code) of the C-terminal tail of wild-type CXCR4, along with the various mutants used in this experiment. B) Sustainment of CXCR4 surface expression from its C-terminal tail-deletion mutant in CD63ΔN-transduced cells. CD63ΔN-transduced MAGIC-5 cells were transfected with CXCR4EGFP, or its C-terminal tail-deletion mutants (d6, d10 or d14), and CXCR4 surface expression and GFP were measured by flow cytometry. Percentage of $GFP^+CXCR4^+$ cells out of total $GFP^+$ cells is shown. Results of one of three, independently conducted, experiments are shown. C) Expression at the plasma membrane was detected for d6, d10 or d14 mutants but not for CXCR4EGFP in the presence of CD63ΔN. CD63ΔN-transduced MAGIC-5 cells transfected with CXCR4EGFP or the mutant DNA, were analyzed by confocal microscopy. Images were acquired through band-pass filters 500–520 nm (GFP: green). Scale bars, 10 μm. DIC images are also shown (lower panel).

in the CD63ΔN-induced suppression? The first question was whether CD63ΔN has any effect on the surface expression of other tetraspanin proteins. The cell surface expression of other tetraspanin proteins such as CD9, CD53, CD81, CD82 and CD151 was not changed in CD63ΔN-transduced MAGIC-5 cells (data not shown) as well as that of CD4, CCR5 and CD71 (Figure 2D). This result suggests that the CD63ΔN-induced suppression might not be caused by any changes of TEMs. The second question was whether other tetraspanin proteins inhibit CXCR4 surface expression. Although CD63wt suppressed CXCR4 surface expression (Figure 2A), we found that CD9, CD81 or CD151 have no suppressive activity on CXCR4 surface expression in MT-4 cells (data not shown). These data strongly suggested that TEMs are not involved in the CD63ΔN-induced suppression. Furthermore, we also found that knockdown of endogenous CD63 resulted in increase of CXCR4 surface expression (Figure 3C). Thus, we deduced that CD63 itself possesses some suppressive ability for CXCR4 surface expression, probably in a TEMs-independent manner.

We next showed that the CD63ΔN-induced disappearance of surface CXCR4 is not because of suppression on gene expression (Figure 4A) or rapid degradation (Figure 4B), but most likely the result of mislocalization of CXCR4. From immunofluorescent analysis and confocal microscopic analysis using phrGFPCXCR4, we found large amounts of intracellular CXCR4 in CD63ΔN-transduced cells but not at the plasma membrane (Figure 4C–E). There have been many reports on the downregulation of cell surface proteins caused by mislocalization. The downregulation of major histocompatibility complex (MHC) class I molecules from the cell surface upon viral infection may be the most well known (30). To evade the monitoring of cytotoxic T lymphocyte, some viral proteins induce mislocalization of MHC class I molecules by many strategies such as (i) rapid internalization, (ii) inhibition of egress from the ER and (iii) re-routing of MHC class I molecules. MHC class I molecules such as human leukocyte antigen (HLA)-A and -B are endocytosed by the HIV Nef and phosphofurin acidic cluster sorting protein-1 in the ARF 6 pathway (31,32). MHC class I molecules (HLA) are prevented from

being transported to the plasma membrane by the adenovirus gene product E3/19K (E19) (33). The re-routing of MHC class I molecules to the lysosome is induced by the human herpesvirus 7 glycoprotein U21 and the mouse cytomegalovirus early gene product (gp48) (34,35).

In the case of CXCR4, rapid internalization was our first guess because CD63 has been reported to play roles in endocytosis of interaction partners such as the HKβ (19) and MT1-MMP (20). Duffield et al. showed that the HKβ interacted with CD63 and the HKβ/CD63 complex was efficiently internalized. When the interaction between CD63 and AP complexes was disrupted, HKβ was not able to be internalized from the cell surface and was retained at the plasma membrane. Takino et al. showed that CD63 formed a complex with MT1-MMP and was involved in internalization, lysosomal targeting and proteolysis of MT1-MMP via LSM-dependent endocytosis (20). These reports suggest that CD63 acts as a mediator between the interaction partners and AP-2 complexes to enhance internalization of the CD63/interaction partner complex (36). In CD63ΔN-transduced cells, however, we could not detect any CXCR4 surface expression for 120 min in anti-CXCR4 mAb feeding experiments under conditions that inhibit actin polymerization (Figure 5A) and found that CD63ΔN-induced suppression of surface CXCR4 expression was not able to be rescued by the dominant negative mutant of dynamin 1 (Figure 5B). Moreover, we found that the CD63ΔN-induced inhibition of X4 HIV infection and suppression of CXCR4 surface expression were not impaired dramatically by LSM deletion (Figures 1E and 2A) and a CD63 mutant lacking LSM (CD63ΔL) still maintained suppressive activity (data not shown). Thus, these data suggest that this CXCR4 down-regulation might not be the result of dynamin-dependent or AP complex-dependent endocytosis. Furthermore, we found that in CD63ΔN-transduced cells, little intracellular CXCR4 was found in the early endosomes (Figure 7A, EEA1). As endocytosed membrane proteins are first collected in the early endosome, this data support the hypothesis that there is little CXCR4 endocytosis in CD63ΔN-transduced cells. Although role of CD63 in these previous studies and that of CD63ΔN in our study appears to be distinct, CD63 has some roles in intracellular trafficking of other proteins.

We showed that intracellular trafficking of CXCR4 via vesicular transport was not stopped by CD63ΔN transduction. The number of CXCR4-containing transport vesicles was not reduced by CD63ΔN transduction (Table 1). We showed that there is no ER retention of CXCR4 in CD63ΔN-transduced cells because the distribution of CXCR4 in CD63ΔN-transduced cells was distinct from that in cells with BFA-induced CXCR4 retention in the ER (Figure 6A). Furthermore, CXCR4 seemed to be distributed in the Golgi of CD63ΔN-transduced cells (Figure 7A,B). This is direct evidence that further rejects the hypothesis that CXCR4 is retained in ER. The fact that a large amount of CXCR4 was also found in the late endosomes/lysosome (Figure 7A,B) indicates the existence of post-Golgi transportation and brings up the possibility that transportation of CXCR4 takes place in CD63ΔN-transduced cells. If lysosome-dependent degradation of CXCR4 indeed takes place in these cells, it should be able to be inhibited by lysosomal inhibitors (CHQ or CMA) treatment. When CD63ΔN-transduced cells were treated with CHX and CHQ or CMA, the degradation of CXCR4 was greatly inhibited (Figure 7C). This biochemical assay confirms the lysosome-dependent degradation of CXCR4, and together with the immunofluorescent analysis, shows that CXCR4 is localized and destroyed in the lysosome.

In this study, we found that six amino acids ($^{347}$SSFHSS$^{352}$) in the CXCR4 C-terminal tail were crucial for the CD63ΔN-induced CXCR4 mislocalization (Figure 9B, C). Some motifs in the CXCR4 C-terminal region such as di-leucine motif ($^{328}$IL$^{329}$) (37) and the integrity of specific serine residues in the C-terminal tail (S$^{324}$, S$^{325}$, S$^{338}$ and S$^{339}$) (7) have been found to be important for localization of CXCR4. However, all the currently known motifs are involved in the internalization of CXCR4.

We also showed that CD63ΔN co-localized with CXCR4 (Figure 8A) and interacted with CXCR4 (Figure 8C). To investigate the importance of this interaction, we assessed whether the resistant mutant in Figure 9 (d6) can associate with CD63ΔN. Deletion of the six amino acids failed to abrogate association with CD63ΔN (data not shown), indicating that these amino acids are not the binding motif for CD63 (CD63ΔN). However, interaction between CXCR4 and CD63ΔN may still be a part of mechanism of changes in CXCR4 trafficking. There may be subtle differences in affinities of wild-type CXCR4 and d6 mutant to CD63ΔN, or CD63ΔN may take CXCR4 to another interacting protein, which binds through the C-terminal amino acids. In fact, direct molecular interaction is not necessary in the case of trafficking regulation of CD19 by another tetraspanin, CD81 (38). CD81 has been reported to have roles in transportation of CD19 to the plasma membrane (36,39,40). Moreover, a series of subsequent studies using many CD81 mutants showed that CD81 plays a variety of roles using different CD81 domains in different cellular compartments (38). CD63 might also have variety of roles in intracellular trafficking. In fact, a large amount of CD63ΔN is in the Golgi (Figure 8B), where more than 35% of total CXCR4 in CD63ΔN-transduced cells was also found (Figures 6C and 7A,B). Since it remains unknown how CXCR4 is sorted in the Golgi, further study is required to understand the mechanism that directs of CXCR4 trafficking at the Golgi apparatus.

In summary, we successfully identified a new X4 HIV-1 entry inhibitor, CD63ΔN. CD63ΔN induced suppression of CXCR4 surface expression, and this phenomenon appears to be caused by mislocalization of CXCR4. Intracellular CXCR4 was distributed not at the plasma membrane but

in intracellular organelles such as the Golgi and the late endosomes/lysosomes and it was degraded in the lysosome. In addition, from CD63-overexpression or depletion experiments, CD63 itself appears to have a role in influencing the level of CXCR4 surface expression, which may be one of its physiological functions.

## Materials and Methods

### Cells and transfection

Human 293T and MAGIC-5 cells (41) and MT-4 cells were maintained as previously described (2). PBMC were prepared from a HIV-1-seronegative donor, and $CD4^+$ cells were isolated using a CD4-positive isolation kit (Dynal Biotech). These cells were stimulated with CD3/CD28 T-cell expander (Dynal) and maintained in RPMI-1640 containing 10% fetal calf serum and 100 U/mL of IL-2. For transfection, Lipofectamin 2000 transfection reagent (Invitrogen), TransIT LT-1 transfection reagent (Takara) or the calcium phosphate method were used. BFA, CMA, CHX and dimethyl sulfoxide (DMSO) were purchased from Sigma and CHQ was purchased from Wako.

### DNA construction

Lentiviral vector DNA, CSII-CDF-GATEWAY-IRES-$H2K^k$, was constructed through the replacement of *hrGFP* with *H-2K*$^k$ (Daiichi Pure Chemicals) in pYK005C (2). *cd63* and *cd63ΔN* was cloned from the human PBL cDNA library into a CMV promoter-driven expression plasmid, pCMV-SPORT6 (Invitrogen). Human *cxcr4* was cloned into pCMV-SPORT6 or an upstream site of *hrgfp* tag in pIRES-hrGFP (Stratagene) (pCXCR4 and phrGFPCXCR4) and pCXCR4 FL GFP, d-6 GFP, d-10 GFP, d-14 GFP (26) were used. *cd63wt*, *cd63ΔN* and *cd63ΔNL*, were cloned into p3XFLAG-CMV-10 (Sigma) and FLAG-tagged *cd63ΔN* was transferred in pCMV-SPORT6. *cxcr4* was cloned into an upstream site of a *halo* tag and downstream of HA tag in pCMV-SPORT6, respectively (pHalo-CXCR4 and pHA-CXCR4). A cDNA on pCMV-SPORT6 was transferred into CSII-CDF-GATEWAY-IRES-$H2K^k$ through BP and LR reaction on Gateway cloning system (Invitrogen). An EGFP-expression *env*-deleted HIV-1 plasmid DNA, pNL-EGFPΔenv, was constructed with a flameshift introduced at the *NheI* site of the *env* in pNLEGFP by blunting and religation. pcDNA3.1(−) HA-Dyn1 K44A (MBA-93) was obtained from ATCC. The nucleotide sequences of all constructs were confirmed using ABI 377 auto-sequencer.

### Antibodies

The following primary unconjugated antibodies against human proteins were used: rat anti-CXCR4 mAbs (A-80, A-145) (42), a mouse anti-CD63 mAb, a goat anti-EEA1 polyclonal antibody (pAb), a mouse anti-LAMP-1 mAb (Santa Cruz Biotechnology), a mouse anti-ERGIC53 mAb (Alexis Biochemicals), a mouse anti-GM130 mAb, a mouse anti-p230 mAb (BD Transduction), a rabbit anti-calnexin pAb (Stressgen Bioreagents), a mouse anti-tubulin mAbs (Sigma) and a mouse anti-β-actin mAb (Cell Signaling Technology). A mouse mAb and a rabbit pAb against FLAG peptides, a mouse mAbs against c-Myc peptides and a horseradish peroxidase (HRP)-conjugated rat mAb against HA peptides were purchased from Sigma, Clontech and Roche, respectively. FITC-conjugated mAbs against CD25 and a phycoerythrin (PE)-conjugated mAb against CCR5 were purchased from BD Pharmingen, FITC or PE-conjugated mouse anti-mouse $H\text{-}2K^k$ mAbs were purchased from Cedarlane and a PE-conjugated mouse mAb against CD4 and FITC-conjugated mAbs against CD71 were purchased from Dako and Immunotech, respectively. Sera from HIV-1-infected people were used for detecting HIV-1 antigens. The following second pAbs were used: an FITC-conjugated goat anti-rat IgG antibody (American Qualex), an Alexa488-conjugated goat anti-mouse IgG pAb (Molecular Probes), Cy5-conjugated donkey pAbs against rabbit IgG, mouse IgG or goat IgG, respectively, a biotin-conjugated donkey anti-rat IgG pAb (Chemicon), a biotin-conjugated goat anti-human IgG pAb (Vector Laboratories) and a HRP-conjugated anti-mouse IgG pAb (Cell Signaling). HRP- (Zymed), PerCP- (BD Bioscience) or Alexa 488- (Molecular Probes)-conjugated streptavidin was also used.

### Small interfering RNA

Synthetic siRNAs directed against *cd63* (no. 199: 5′-ACAGCUUGUCCUGAGUCAGACCAUA-3′, no. 317: 5′-GCCUGCAAGGAGAACUAUUGUCUUA-3′ and no. 844: 5′-GAGUGGAAUAGUAUCCUCCAGGUUU-3′) and Stealth RNAi Negative Control Duplexes Medium GC Duplex were purchased from Invitrogen. Transfection was performed using Lipofectamine 2000.

### Flow cytometric analysis

Flow cytometric analyses using cell line were performed as previously described (2). In case of T-cells staining, Fc receptor blocker (Dynal) was used. Data was collected using FACScan or FACScalibur (BD Bioscience) and analyzed using WinMDI software.

### Immunoprecipitations and Western blotting

CXCR4 was detected as previously described (42). To detect FLAG-tagged protein, cells were scraped in triple detergent containing 1% Igepal (Sigma), 0.1% SDS, 0.5% sodium deoxycholate in 20 mM Tris–HCl (pH 8) – 0.15 M NaCl – protease inhibitor cocktail Complete (Roche). For samples of deglycosylation procedure, immunoprecipitation was required. After supplementation of an anti-FLAG mAb and incubation for 12 h at 4°C in the presence of protein G-sepharose (Amersham Biosciences), immunoprecipitants were treated with Glycoprotein Deglycosylation Kit (Calbiochem) according to the manufacturer's protocol. Interaction between CD63 and CXCR4 was also detected as described above except detergent buffer, instead of triple detergent, single detergent containing 1% Triton X-100 in 50 mM Tris–HCl (pH 8) – 0.15 M NaCl – protease inhibitor cocktail Complete, was used. Immunoprecipitation and immunoblotting of MT1-MMP were carried out as previously described (20). For degradation assay, cells transfected with pHA-CXCR4 were incubated in the presence of 15 μg/mL CHX with either 50 μg/mL CHQ, 20 μg/mL CMA or vehicle control (DMSO) and harvested at the indicated times. Cells were lysed with single detergent.

### HIV-1 infection

Lentiviral vector and HIV-1 preparation were carried out as described previously (2). Cells transduced with the original, CD63 mutant fragments (clone 12.03 and clone 12.22) were infected with $HIV\text{-}1_{NL4\text{-}3}$ and expression of HIV-1 antigen was examined 4 dpi using an anti-HIV-1 human serum. CD63wt or CD63 mutant-transduced cells were infected with NL-EGFP (24) at a MOI of 0.1. Three dpi, dual color flow cytometric analysis was performed. To prepare amphotropic MLV Env-pseudotyped HIV-1, 293T cells were co-transfected with pNL4-3Δenv and pJD-1 (43). Forty-eight hours later, culture supernatants were collected and used for infection. CD63ΔN-transduced cells were infected with $HIV\text{-}1_{NL4\text{-}3}$ or $HIV\text{-}1_{JR\text{-}CSF}$ (44) at a MOI of 2 and then the culture supernatant was harvested. The level of HIV-1 $p24^{gag}$ antigen was measured by ELISA (ZeptoMetrix Corp.). To detect HIV-1 DNA by polymerase chain reaction (PCR), cells were harvested 1 dpi and PCR was performed with HIV *Tat/Rev*-specific primers (45). To prepare heat inactivated HIV-1 as a negative control, viruses were incubated at 65°C for 30 min.

### Chemotaxis assay

Cell migration was assayed in 24-well cell culture chambers using inserts with 8 μm pore membrane (Falcon). Membranes were pre-coated with fibronectin. Buffer including 100 nM of SDF-1 (Wako) and SYTO 24 (Molecular Probes), and MAGIC-5 cells resuspended in OPTI-MEM reduced-serum medium (Gibco) were applied on lower well and upper wells, respectively. After incubation for 12 h, cells on lower surface of the membrane were visualized by SYTO 24 and counted using a fluorescent microscope in three different fields.

### Microscopic analyses

For live cell imaging, cells grown on 12-mm glass-bottomed culture dishes (Iwaki) were transfected with appropriate DNA, at 48 h post-transfection stained with HaloTag™-ligand (Promega), NBD $C_5$-ceramide (Molecular

Probes), Hoechst33342 (Hoechst) or LysoTracker Blue DND-22 (Molecular Probes) according to manufacturer protocols. To detect surface CXCR4 on live cells, cells were incubated with an anti-CXCR4 mAb (A-145) for 30 min at 4°C. In mAb feeding experiments, cells were cultured in medium containing an FITC-conjugated anti-CXCR4 mAb (A-145) and Hoechst, in the presence or absence of 5 μM of cytochalasin D (Sigma). To detect CXCR4, CD63 or FLAG-tagged proteins, cells grown on APS-coated slide glasses (Matsunami) were fixed in 4% (v/v) paraformaldehyde (PFA) for 60 min at 4°C. After washing with PBS, cells were blocked with PBS containing 10% normal donkey serum, followed by an overnight incubation with primary Abs at 4°C. After extensive washing with PBS, cells were incubated with the secondary Abs for 60 min. In case of dual staining, we routinely incubate cells with no, or only one primary Ab, which were served as control for non-specific binding of secondary Abs. To detect CD63, intracellular CXCR4 with intracellular organelle markers or FLAG-tagged CD63ΔN, cells were treated with PBS containing 0.05% saponin for 10 min at room temperature after fixation to enhance permeability. Cells were analyzed at 37°C (live cells) or room temperature (fixed cells) using a 63×/ 1.4-0.60 HCX PL APO objective on a DMIRE2-TCS SP2 AOBS confocal microscope system (both from Leica) or a PLAPON 60× O TIRFM objective on a IX71 TIRF microscope system (all from Olympus). Images were acquired and analyzed using LCS 2.61 (Leica) or Basic Metamorph (Molecular Devices) and processed using Photoshop CS2 (Adobe).

### *Statistical analysis*

The Mann–Whitney's *U*-test and Student's *t*-test were used to determine statistical significance, and $P < 0.05$ was considered significant.

## Acknowledgments

We thank the many colleagues who have contributed ideas and help to this project, in particular Naoko Misawa, Kuniko Hieda and Shunsuke Hatta for technical support, Chuanyi Nie for discussion, Prof. Kouji Matsushima for providing CXCR4 plasmid DNA, Prof. Hiroshi Sato for providing Myc-MT1-MMP plasmid DNA and Prof. Hiroshi Kimura for teaching us to manipulate TIRFM. The authors declare no competing financial interests. This work was supported by grants from the Ministry of Health, Labor, and Welfare and the Ministry of Education, Culture, Sports, Science and Technology of JAPAN. T. Y. is a research fellow of the Japan Society for the Promotion of Science.

## Supplementary Materials

**Figure S1: Nucleotide sequence of *cd63* cDNA.** Nucleotide sequences of the wild-type *cd63* cDNA, and that of the cDNA clones (12.03 and 12.22) isolated at the outset of this study and newly cloned cDNA for preparing lentiviral vector, are indicated. Capital letters indicate the translated region (the CD63wt ORF starts at +95 and the CD63ΔN ORF starts at +341). Dashed lines indicate positions showing identical nucleotide sequence to the human *cd63* cDNA in the NCBI database (accession number of human *cd63* cDNA, NM_001780).

**Figure S2: Subcellular distribution of CXCR4 in empty vector-transduced cells.** Co-localization of CXCR4 with intracellular organelles (calnexin; ER, GM130; *cis*-Golgi, LAMP-1; late endosome) was shown in empty vector-transduced MAGIC-5 cells. Images were acquired through band-pass filters (BPF) 500–520 nm (CXCR4: green) and BPF 650–700 nm (intracellular organelles: magenta). Scale bars, 10 μm. Merged images are shown in bottom.

Supplementary experimental procedures: Microscopic analyses.

Supplemental materials are available as part of the online article at http://www.blackwell-synergy.com

## References

1. Goff SP. Retrovirus restriction factors. Mol Cell 2004;16:849–859.
2. Kawano Y, Yoshida T, Hieda K, Aoki J, Miyoshi H, Koyanagi Y. A lentiviral cDNA library employing lambda recombination used to clone an inhibitor of human immunodeficiency virus type 1-induced cell death. J Virol 2004;78:11352–11359.
3. Feng Y, Broder CC, Kennedy PE, Berger EA. HIV-1 entry cofactor: functional cDNA cloning of a seven-transmembrane, G protein-coupled receptor. Science 1996;272:872–877.
4. Oberlin E, Amara A, Bachelerie F, Bessia C, Virelizier JL, Arenzana-Seisdedos F, Schwartz O, Heard JM, Clark-Lewis I, Legler DF, Loetscher M, Baggiolini M, Moser B. The CXC chemokine SDF-1 is the ligand for LESTR/fusin and prevents infection by T-cell-line-adapted HIV-1. Nature 1996;382:833–835.
5. Signoret N, Oldridge J, Pelchen-Matthews A, Klasse PJ, Tran T, Brass LF, Rosenkilde MM, Schwartz TW, Holmes W, Dallas W, Luther MA, Wells TN, Hoxie JA, Marsh M. Phorbol esters and SDF-1 induce rapid endocytosis and down modulation of the chemokine receptor CXCR4. J Cell Biol 1997;139:651–664.
6. Cheng ZJ, Zhao J, Sun Y, Hu W, Wu YL, Cen B, Wu GX, Pei G. Beta-arrestin differentially regulates the chemokine receptor CXCR4-mediated signaling and receptor internalization, and this implicates multiple interaction sites between beta-arrestin and CXCR4. J Biol Chem 2000;275:2479–2485.
7. Orsini MJ, Parent JL, Mundell SJ, Benovic JL, Marchese A. Trafficking of the HIV coreceptor CXCR4. Role of arrestins and identification of residues in the c-terminal tail that mediate receptor internalization. J Biol Chem 1999;274:31076–31086.
8. Marchese A, Benovic JL. Agonist-promoted ubiquitination of the G protein-coupled receptor CXCR4 mediates lysosomal sorting. J Biol Chem 2001;276:45509–45512.
9. Marchese A, Raiborg C, Santini F, Keen JH, Stenmark H, Benovic JL. The E3 ubiquitin ligase AIP4 mediates ubiquitination and sorting of the G protein-coupled receptor CXCR4. Dev Cell 2003;5:709–722.
10. Neel NF, Schutyser E, Sai J, Fan GH, Richmond A. Chemokine receptor internalization and intracellular trafficking. Cytokine Growth Factor Rev 2005;16:637–658.
11. Tarrant JM, Robb L, van Spriel AB, Wright MD. Tetraspanins: molecular organisers of the leukocyte surface. Trends Immunol 2003;24:610–617.
12. Escola JM, Kleijmeer MJ, Stoorvogel W, Griffith JM, Yoshie O, Geuze HJ. Selective enrichment of tetraspan proteins on the internal vesicles of multivesicular endosomes and on exosomes secreted by human B-lymphocytes. J Biol Chem 1998;273:20121–20127.
13. Kobayashi T, Vischer UM, Rosnoblet C, Lebrand C, Lindsay M, Parton RG, Kruithof EK, Gruenberg J. The tetraspanin CD63/lamp3 cycles between endocytic and secretory compartments in human endothelial cells. Mol Biol Cell 2000;11:1829–1843.
14. Metzelaar MJ, Wijngaard PL, Peters PJ, Sixma JJ, Nieuwenhuis HK, Clevers HC. CD63 antigen. A novel lysosomal membrane glycoprotein, cloned by a screening procedure for intracellular antigens in eukaryotic cells. J Biol Chem 1991;266:3239–3245.
15. Rous BA, Reaves BJ, Ihrke G, Briggs JA, Gray SR, Stephens DJ, Banting G, Luzio JP. Role of adaptor complex AP-3 in targeting wild-type and mutated CD63 to lysosomes. Mol Biol Cell 2002;13:1071–1082.
16. Berditchevski F, Tolias KF, Wong K, Carpenter CL, Hemler ME. A novel link between integrins, transmembrane-4 superfamily proteins (CD63 and CD81), and phosphatidylinositol 4-kinase. J Biol Chem 1997;272:2595–2598.
17. Jung KK, Liu XW, Chirco R, Fridman R, Kim HR. Identification of CD63 as a tissue inhibitor of metalloproteinase-1 interacting cell surface protein. EMBO J 2006;25:3934–3942.

18. Latysheva N, Muratov G, Rajesh S, Padgett M, Hotchin NA, Overduin M, Berditchevski F. Syntenin-1 is a new component of tetraspanin-enriched microdomains: mechanisms and consequences of the interaction of syntenin-1 with CD63. Mol Cell Biol 2006;26:7707–7718.
19. Duffield A, Kamsteeg EJ, Brown AN, Pagel P, Caplan MJ. The tetraspanin CD63 enhances the internalization of the H,K-ATPase beta-subunit. Proc Natl Acad Sci U S A 2003;100:15560–15565.
20. Takino T, Miyamori H, Kawaguchi N, Uekita T, Seiki M, Sato H. Tetraspanin CD63 promotes targeting and lysosomal proteolysis of membrane-type 1 matrix metalloproteinase. Biochem Biophys Res Commun 2003;304:160–166.
21. Levy S, Shoham T. The tetraspanin web modulates immune-signalling complexes. Nat Rev Immunol 2005;5:136–148.
22. Hemler ME. Tetraspanin functions and associated microdomains. Nat Rev Mol Cell Biol 2005;6:801–811.
23. Stipp CS, Kolesnikova TV, Hemler ME. Functional domains in tetraspanin proteins. Trends Biochem Sci 2003;28:106–112.
24. Miura Y, Misawa N, Kawano Y, Okada H, Inagaki Y, Yamamoto N, Ito M, Yagita H, Okumura K, Mizusawa H, Koyanagi Y. Tumor necrosis factor-related apoptosis-inducing ligand induces neuronal death in a murine model of HIV central nervous system infection. Proc Natl Acad Sci U S A 2003;100:2777–2782.
25. Endres MJ, Clapham PR, Marsh M, Ahuja M, Turner JD, McKnight A, Thomas JF, Stoebenau-Haggarty B, Choe S, Vance PJ, Wells TN, Power CA, Sutterwala SS, Doms RW, Landau NR et al. CD4-independent infection by HIV-2 is mediated by fusin/CXCR4. Cell 1996;87:745–756.
26. Futahashi Y, Komano J, Urano E, Aoki T, Hamatake M, Miyauchi K, Yoshida T, Koyanagi Y, Matsuda Z, Yamamoto N. Separate elements are required for ligand-dependent and -independent internalization of metastatic potentiator CXCR4. Cancer Sci 2007;98:373–379.
27. von Lindern JJ, Rojo D, Grovit-Ferbas K, Yeramian C, Deng C, Herbein G, Ferguson MR, Pappas TC, Decker JM, Singh A, Collman RG, O'Brien WA. Potential role for CD63 in CCR5-mediated human immunodeficiency virus type 1 infection of macrophages. J Virol 2003;77:3624–3633.
28. Ho SH, Martin F, Higginbottom A, Partridge LJ, Parthasarathy V, Moseley GW, Lopez P, Cheng-Mayer C, Monk PN. Recombinant extracellular domains of tetraspanin proteins are potent inhibitors of the infection of macrophages by human immunodeficiency virus type 1. J Virol 2006;80:6487–6496.
29. Jourdan P, Abbal C, Noraz N, Hori T, Uchiyama T, Vendrell JP, Bousquet J, Taylor N, Pene J, Yssel H. IL-4 induces functional cell-surface expression of CXCR4 on human T cells. J Immunol 1998;160:4153–4157.
30. Hewitt EW. The MHC class I antigen presentation pathway: strategies for viral immune evasion. Immunology 2003;110:163–169.
31. Schwartz O, Marechal V, Le Gall S, Lemonnier F, Heard JM. Endocytosis of major histocompatibility complex class I molecules is induced by the HIV-1 Nef protein. Nat Med 1996;2:338–342.
32. Piguet V, Wan L, Borel C, Mangasarian A, Demaurex N, Thomas G, Trono D. HIV-1 Nef protein binds to the cellular protein PACS-1 to downregulate class I major histocompatibility complexes. Nat Cell Biol 2000;2:163–167.
33. Andersson M, Paabo S, Nilsson T, Peterson PA. Impaired intracellular transport of class I MHC antigens as a possible means for adenoviruses to evade immune surveillance. Cell 1985;43:215–222.
34. Hudson AW, Howley PM, Ploegh HL. A human herpesvirus 7 glycoprotein, U21, diverts major histocompatibility complex class I molecules to lysosomes. J Virol 2001;75:12347–12358.
35. Reusch U, Muranyi W, Lucin P, Burgert HG, Hengel H, Koszinowski UH. A cytomegalovirus glycoprotein re-routes MHC class I complexes to lysosomes for degradation. EMBO J 1999;18:1081–1091.
36. Berditchevski F, Odintsova E. Tetraspanins as regulators of protein trafficking. Traffic 2007;8:89–96.
37. Signoret N, Rosenkilde MM, Klasse PJ, Schwartz TW, Malim MH, Hoxie JA, Marsh M. Differential regulation of CXCR4 and CCR5 endocytosis. J Cell Sci 1998;111:2819–2830.
38. Shoham T, Rajapaksa R, Kuo CC, Haimovich J, Levy S. Building of the tetraspanin web: distinct structural domains of CD81 function in different cellular compartments. Mol Cell Biol 2006;26:1373–1385.
39. Maecker HT, Levy S. Normal lymphocyte development but delayed humoral immune response in CD81-null mice. J Exp Med 1997;185:1505–1510.
40. Miyazaki T, Muller U, Campbell KS. Normal development but differentially altered proliferative responses of lymphocytes in mice lacking CD81. EMBO J 1997;16:4217–4225.
41. Hachiya A, Aizawa-Matsuoka S, Tanaka M, Takahashi Y, Ida S, Gatanaga H, Hirabayashi Y, Kojima A, Tatsumi M, Oka S. Rapid and simple phenotypic assay for drug susceptibility of human immunodeficiency virus type 1 using CCR5-expressing HeLa/CD4(+) cell clone 1-10 (MAGIC-5). Antimicrob Agents Chemother 2001;45:495–501.
42. Tanaka R, Yoshida A, Murakami T, Baba E, Lichtenfeld J, Omori T, Kimura T, Tsurutani N, Fujii N, Wang ZX, Peiper SC, Yamamoto N, Tanaka Y. Unique monoclonal antibody recognizing the third extracellular loop of CXCR4 induces lymphocyte agglutination and enhances human immunodeficiency virus type 1-mediated syncytium formation and productive infection. J Virol 2001;75:11534–11543.
43. Dougherty JP, Wisniewski R, Yang SL, Rhode BW, Temin HM. New retrovirus helper cells with almost no nucleotide sequence homology to retrovirus vectors. J Virol 1989;63:3209–3212.
44. Kawano Y, Tanaka Y, Misawa N, Tanaka R, Kira JI, Kimura T, Fukushi M, Sano K, Goto T, Nakai M, Kobayashi T, Yamamoto N, Koyanagi Y. Mutational analysis of human immunodeficiency virus type 1 (HIV-1) accessory genes: requirement of a site in the nef gene for HIV-1 replication in activated CD4+ T cells in vitro and in vivo. J Virol 1997;71:8456–8466.
45. Zack JA, Arrigo SJ, Weitsman SR, Go AS, Haislip A, Chen IS. HIV-1 entry into quiescent primary lymphocytes: molecular analysis reveals a labile, latent viral structure. Cell 1990;61:213–222.

Human Immunology (2008) 69, 533-542

ELSEVIER

ASHI AMERICAN SOCIETY FOR HISTOCOMPATIBILITY & IMMUNOGENETICS www.ashi-hla.org

journal homepage: www.elsevier.com/locate/humimm

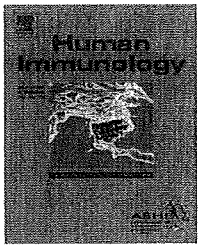

# Rapid induction of OX40 ligand on primary T cells activated under DNA-damaging conditions

Kayo Kondo[a], Kazu Okuma[a], Reiko Tanaka[a], Goro Matsuzaki[b], Aftab A. Ansari[c], Yuetsu Tanaka[a,*]

[a] *Department of Immunology, Graduate School of Medicine, University of the Ryukyus, Okinawa, Japan*
[b] *Molecular Microbiology Group, Center of Molecular Biosciences, University of the Ryukyus, Okinawa, Japan*
[c] *Department of Pathology, Emory University School of Medicine, Atlanta, GA, USA*

Received 12 May 2008; received in revised form 2 July 2008; accepted 9 July 2008

**KEYWORDS**
Human OX40L;
Activated T cells;
DNA stress;
Costimulation;
Senescence

**Summary** We have previously demonstrated that normal human T cells either long-term repeatedly stimulated or freshly activated *in vitro* in the presence of TGF-$\beta$ express the cell surface T-cell costimulating molecule OX40 ligand (OX40L). To further elucidate the kinetics of OX40L expression by human T cells, we have examined whether cell proliferation was required for the expression of OX40L. Thus, normal fresh peripheral blood mononuclear cells were stimulated with immobilized anti-CD3 antibody in the presence of the DNA synthesis-blocking agents such as mitomycin C, 5-fluorouracil, or X-ray irradiation. Flow cytometric analyses demonstrated that a significant frequency of these DNA-damaged activated primary $CD4^+$ and $CD8^+$ T cells became $OX40L^+$ as early as 1 hour after treatment. The OX40L induction on the DNA-damaged activated T cells was inhibited by treatment with either RNA or protein synthesis inhibitors, actinomycin D, or cycloheximide, respectively. Induced OX40L on T cells was functional because it bound recombinant OX40. These data indicate that human primary T cells are programmed to rapidly express functional OX40L molecules after stimulation under DNA-damaging conditions, demonstrating that the induction of OX40L by T cells is independent of cell proliferation. The clinical implications of these new findings are discussed.


## Introduction

Human OX40 ligand (OX40L) was first described by our laboratory as a gp34 molecule that is preferentially expressed on the cell surface of human T-cell lines transformed by human T-cell leukemia virus type I using a monoclonal antibody (mAb) [1]. Subsequently, gp34 was cloned [2] and finally identified as a member of the tumor necrosis factor (TNF) superfamily (TNFSF) [3]. OX40, its cognate receptor, was originally reported by Paterson *et al.* [4] as a cell surface antigen expressed by rat $CD4^+$ T-cell blasts that was recognized by MRC OX-40 antibody. OX40 is a member of the TNF receptor superfamily, which includes molecules such as Fas, CD27, CD30, CD40, 4-1BB, and others [4]. OX40 is transiently expressed on the cell surface of activated T cells [5]. The

* Corresponding author. Fax: +81-98-895-1437.
*E-mail address:* yuetsu@s4.dion.ne.jp (Y. Tanaka).

0198-8859/$ -see front matter © 2008 American Society for Histocompatibility and Immunogenetics. Published by Elsevier Inc. All rights reserved.
doi:10.1016/j.humimm.2008.07.001

**ABBREVIATIONS**

| | |
|---|---|
| 5-FU | 5-fluorouracil |
| Act-D | actinomycin D |
| CHX | cycloheximide |
| CsA | cyclosporine A |
| DC | dendritic cell |
| ELISA | enzyme-linked immunosorbent assay |
| FCM | flow cytometry |
| IgG | immunoglobulin G |
| IL | interleukin |
| i.p. | intraperitoneally |
| mAb | monoclonal antibody |
| MMC | mitomycin C |
| NK | natural killer |
| OX40L | OX40 ligand |
| PBMCs | peripheral blood mononuclear cells |
| PBS | phosphate-buffered saline |
| sOX40 | soluble human OX40 |
| TCR | T-cell receptor |
| TGF-$\beta$1 | transforming growth factor-$\beta$1 |
| Th1 | T helper 1 |
| TNF | tumor necrosis factor |
| TNFSF | tumor necrosis factor superfamily |
| UV | ultraviolet |

coexpression of OX40L and OX40 has been reported to be critical for T-cell response, which includes proliferation, survival, cytokine production, and the generation of memory cells [6,7] in a tumor necrosis factor associated factor (TRAF)2- and survival-dependent manner [8]. The delineation of the crystal structure of the OX40-OX40L complex demonstrated that whereas OX40L is a very compact, brick-shape structure that packs together to form flower-like trimers, the OX40 molecule binds at the monomer to monomer interface [9].

Initially, under normal conditions, the expression of OX40L was thought to be restricted to antigen-presenting cells such as dendritic cells (DCs) and B cells that were activated by ligation of the CD40L molecule or surface Ig [10,11], as well as select non-antigen-presenting cells such as endothelial cells [12]. OX40L expression by DCs was also induced by thymic stromal lymphopoietin [13]. It is, however, now becoming clear that functional OX40L can be induced on a wide variety of cells including activated T cells [14], natural killer (NK) cells [15], and mast cells [16], highlighting the multicell lineage expression of the OX40L molecule. It is reasoned that OX40-induced T-cell costimulation in fact occurs quite frequently via OX40-OX40L interaction at sites of inflammation, resulting in modulation of immune responses. Indeed, T-T-cell interactions during late stages of T-cell responses via OX40 and OX40L have been implicated in the long-term survival of antigen-specific $CD4^+$ memory effector T cells in the murine system [14]. It is of interest to note that whereas ligation of human OX40 by human OX40L stimulates human $OX40^+$ T cells, under Th1 conditions such OX40 stimulation by OX40L appears to result in the apoptosis of $CD4^+$ T cells [17]. Thus, it has been suggested that interactions between OX40L-OX40 control the fate of T-cell responses as a double-edge effector.

Recently, we reported that a high frequency of normal human T cells express functional OX40L when they were either long-term repeatedly stimulated *in vitro* or primarily stimulated once with anti-CD3 antibody in the presence of transforming growth factor $\beta$1 (TGF-$\beta$1) [18]. These observations prompted us to determine whether cell proliferation was necessary for the induction of OX40L on activated T cells. Thus, in the present study, we examined the effects of DNA synthesis-inhibiting agents on OX40L expression by fresh T cells activated via T-cell receptor (TCR) with immobilized anti-CD3 antibody. We report herein that lymphocytes including $CD4^+$ T and $CD8^+$ T cells express OX40L following a short-term period independent of cell proliferation, but dependent on both RNA and protein syntheses and activation.

## Subjects and methods

### Reagents

The medium used throughout these studies included RPMI 1640 medium (Sigma, St. Louis, MO) supplemented with 5% heat-inactivated fetal calf serum (Sigma; referred to as RPMI medium). Human recombinant cytokines used were interleukin (IL)-2 and TGF-$\beta$1 purchased from Peprotech (London, UK). The fluorescent mAbs used and their vendors are listed in parentheses. These included antihuman CD4, CD8, CD19, CD40, CD154, HLA-DR, and CD25 (Beckman-Coulter, Fullerton, CA), antihuman CD70 (CD27L) (Ancell, Bayport, MN), antihuman 4-1BB, 4-1BBL, TNF-$\alpha$, and CD30 (BD Biosciences, Teterboro, NJ), antihuman Fas ligand (MBL Nagoya, Japan), antihuman TRAIL, CD30L, GITRL, CTLA-4, and GITR (R&D Systems, Inc., Minneapolis, MN), and OKT-3 and anti-HLA class I [W6/32, American Type Culture Collection (ATCC); ATCC, VA].

The mAbs produced in our laboratory included a mouse IgG1 anti-OX40L (clone 5A8) [19]; mouse IgG1 anti-human OX40 (clone B-7B5) [20]; and rat IgG2b anti-OX40 (clone W4-54, which was generated from a WKA rat and capable of blocking OX40/OX40L interaction) [18]. These in-house mAbs were purified from SCID mouse ascites fluids by gel filtration and labeled using FITC, POD, and Cy5 using commercial labeling kits according to the manufacturer's instructions. Biotinylated recombinant soluble human OX40 (sOX40, a form of murine IgG2a-Fc fusion protein) and OX40L (sOX40L, a form of murine CD8-fusion protein) were purchased from Ancell. Mitomycin C (MMC) was purchased from Kyowahakko (Tokyo, Japan). Actinomycin D (Act-D), 5-fluorouracil (5-FU), cycloheximide (CHX), cyclosporine A (CsA), and $H_2O_2$ were purchased from Wako Pure Chemical Industries (Osaka, Japan). Metalloproteinase inhibitor (KB8301) for Fas-L detection was purchased from BD Pharmingen.

### Enzyme-linked immunosorbent assay (ELISA)

The ELISA kits utilized for the quantitation of human OX40L and OX40 were generated by our laboratory using combinations of in-house capture and detector mAbs. The detector mAbs were labeled utilizing a POD kit (Dojin, Kumamoto, Japan) according to the manufacturer's instructions. For standards, soluble human OX40L-murine CD8 fusion protein and human OX40-murine Ig (Ancell) were used. The weight ratio of OX40L and OX40 in the fusion proteins was calculated to be 46 and 42%, respectively, based on the published amino acid sequences of the molecules.

### Stimulation of T cells *in vitro*

Human peripheral blood mononuclear cells (PBMCs) were stimulated with anti-CD3 antibody (OKT-3) as described previously [18]. Briefly, PBMCs obtained by density gradient centrifugation on HistoPAQUE-1077 (Sigma) were suspended at $1 \times 10^6$ cells/ml in RPMI medium supplemented with 20 U/ml IL-2. The PBMCs were dispensed into individual wells of 24-well plates (BD Pharmingen) (1 ml/well) that had been precoated with anti-CD3 mAb. The PBMCs were cultured for 1 to 72 hours at 37°C in a 5% $CO_2$ humidified atmosphere in the presence or absence of MMC, Act-D, CHX, CsA, or TGF-$\beta$1, alone or in combination. In some experiments, PBMCs were pretreated with 50 $\mu$g/ml MMC for 45 minutes at 37°C, X-ray irradiated by exposure to a Hitachi MBR-1505R2, or UV-A or UV-B irradiated using SLUV-4 254/360 nm (AS ONE, Osaka, Japan). The UV dose was measured using a UV meter (UVP, Inc., Upland, CA). Cell viability was determined after an aliquot of the cells was stained with 0.1% eosin-Y. An anti-OX40 blocking mAb (W4-54) [18] was used to prevent the intercellular interaction between OX40 and OX40L [21]. For the quantitation of levels of OX40L and OX40 in the cells, cell lysates were prepared using a low-salt extraction buffer [1].

### Flow cytometry (FCM)

FCM was carried out as described previously [18]. Briefly, cells to be analyzed were Fc-blocked by incubation of the cells with 2 mg/ml normal human pooled IgG on ice for 15 minutes. Aliquots of these cells were then subjected to staining using predetermined optimum concentrations of dye-conjugated mAbs for 30 minutes on ice. The cells were then washed using FACS buffer [phosphate-buffered saline (PBS) containing 2% fetal calf serum and 0.1% sodium azide], fixed in 1% paraformaldehyde (PFA)-containing FACS buffer, and analyzed using a FACSCalibur, and the data obtained were analyzed using Cell Quest software (BD Pharmingen). To determine whether cell surface OX40L is functional, Fc-blocked cells were incubated with biotinylated recombinant sOX40 at a concentration of 2.5 $\mu$g/ml for 30 minutes on ice, followed by staining with PE-labeled streptavidin (Beckman Coulter) for 30 minutes on ice, and then analyzed by FCM.

In all the FCM analyses, isotype controls were used, and dead cells were gated out according to the forward and side scatter profile. In the appropriate experiments, samples were stained in conjunction with propidium iodide to exclude dead cells.

### Animal studies

The immunodeficient BALB/c-Rag2$^{-/-}\gamma_c^{-/-}$ (referred to as BRG) mice [22] were obtained from Dr. M. Ito at the Central Institute for Experimental Animals (Kanagawa, Japan). Fresh human PBMCs ($1 \times 10^7$ cells/head) were inoculated intraperitoneally (i.p.) into BRG mice, immediately followed by either MMC (620 $\mu$g/ head) or PBS inoculation. After 24 hours, the mice were sacrificed, and the cells harvested from the peritoneal cavity were pooled with spleen cells and aliquots subjected to phenotypic analysis by FCM. Multicolor analysis of the human cells was performed based on gating on cells expressing HLA class I.

## Results

### Induction of OX40L expression on T cells activated under DNA-damaging conditions

To test whether cell proliferation was required for the expression of OX40L by T cells, aliquots of fresh PBMCs were treated with either medium or a representative DNA synthesis inhibitor drug, MMC, and then stimulated *in vitro* with immobilized anti-CD3 mAb for 3 days. Aliquots of PBMCs cultured in the presence of TGF-$\beta$ were used for the purposes of positive control for the expression of OX40L. As illustrated in Figure 1a, a significant number of MMC-treated cells within the lymphocyte gate were positive for OX40L. The percentage of OX40L-expressing cells treated with MMC was four times greater than the PBMCs stimulated in the presence of TGF-$\beta$1. PBMCs treated with MMC and stimulated with anti-CD3 in the presence of TGF-$\beta$ did not demonstrate any further increase in the frequency of the OX40L$^+$ lymphocytes. Approximately two thirds of the OX40L-positive MMC-treated lymphocytes were also OX40 positive (Figure 1a), indicating that both OX40L and OX40 are coexpressed by cells activated in the presence of a DNA-damaging agent, as we have previously demonstrated for long-term cultured T cells [18]. Thus, it is clear that cell proliferation is not necessary for the expression of OX40L on activated human lymphocytes. As far as we know, the present data are the first to demonstrate that an inhibitor of DNA synthesis induces the cell surface expression of OX40L following TCR-mediated activation of human lymphocytes.

To determine which lymphocyte subsets expressed OX40L in these MMC-treated *in vitro* anti-CD3 activated PBMCs, dual-color staining was performed on lymphocytes gated according to forward and side scatter profiles. Figure 1b illustrates that OX40L was expressed predominantly by both CD4$^+$ and CD8$^+$ T cells and a minor (10%) population of lymphocytes expressing CD19 (B cells). No detectable induction of OX40L was observed on CD56$^+$ NK or CD14$^+$ monocytes (data not shown) under the present conditions.

To exclude the possibility that T cells become OX40L$^+$ through activation via their Fc receptors that may be ligated by the immunoglobulin G (IgG) Fc region of plate-bound anti-CD3 mAb, as has been demonstrated for human NK cells that were activated via the Fc-$\gamma$ receptor CD16 [15], three additional agents that induce cell activation were utilized. These included the use of phytohemagglutinin A, phorbol 12-myristate 13-acetate (PMA), and immunobeads conjugated with anti-CD3/anti-CD28. As illustrated in Figure 1c, all three agents induced the expression of OX40L on the MMC-treated T cells but to varying degrees. Figure 1c also illustrates that among these agents, the CD3/CD28 mAb-conjugated beads were the most potent and PMA was the least potent in their ability to induce not only OX40L but also OX40 following MMC treatment of T cells, suggesting an indirect CD28 involvement for the induction of OX40L and OX40.

In efforts to determine whether the inhibition of DNA synthesis was effective in OX40L induction by not only primary T cells but also previously stimulated T cells, normal human T cells stimulated once with anti-CD3 mAb were restimulated either in the presence or in the absence of MMC for 1 day and then OX40L expression was analyzed. As illustrated in Figure 1d, MMC treatment increased the percentage of OX40L$^+$ cells from 20 to 51% of the restimulated T cells, demonstrating that both fresh and previously activated T cells were susceptible to OX40L induction by activation under DNA synthesis-inhibiting conditions.

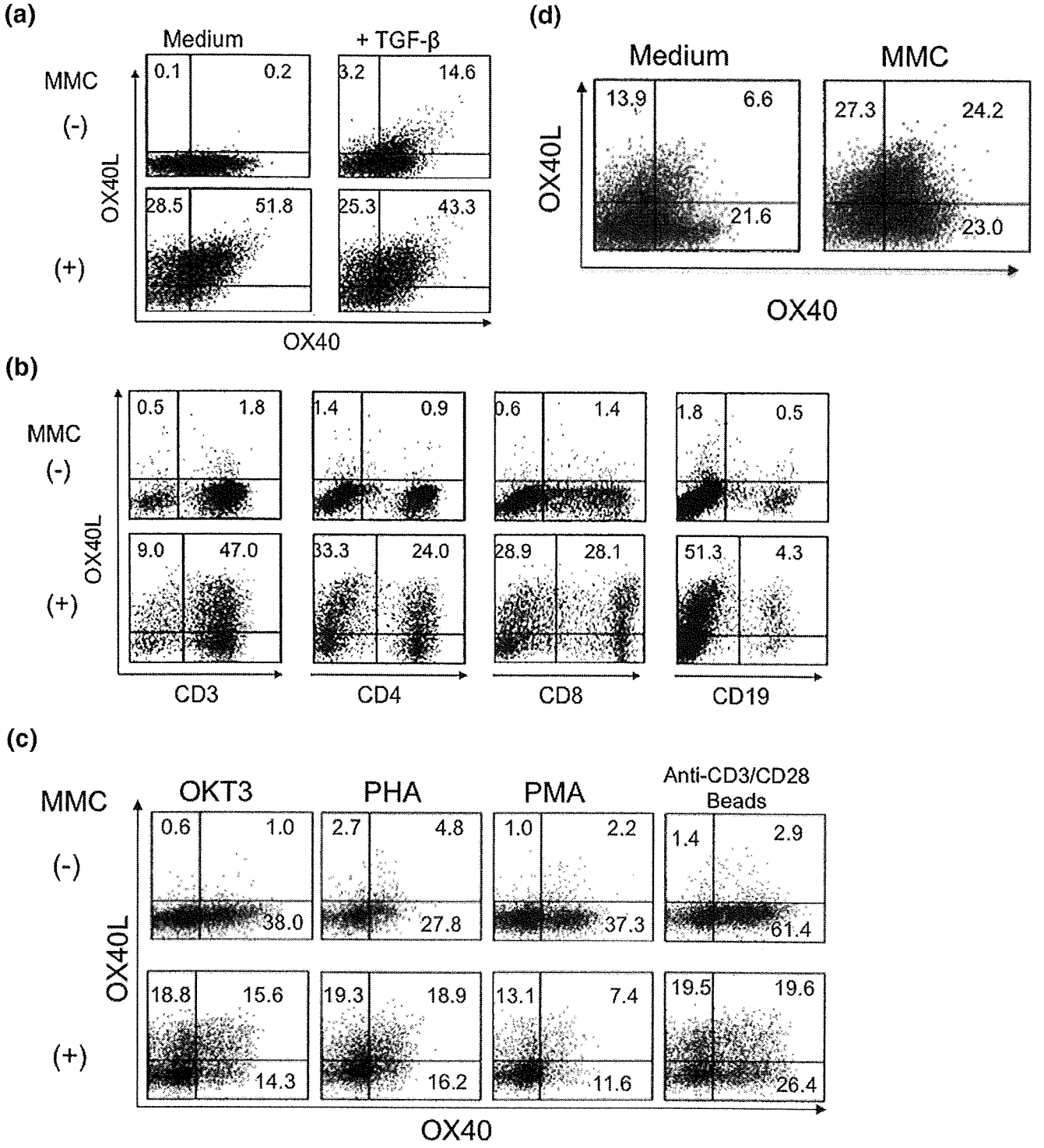


**Figure 1.** Induction of cell surface OX40L by primary T cells by MMC treatment and cell activation. (a) Fresh PBMCs were either untreated or pretreated with MMC (50 μg/ml for 45 minutes at 37°C), stimulated with immobilized OKT-3 in the presence or absence of 20 ng/ml TGF-β1 for 3 days, and then examined for OX40L and OX40 expression by FCM. (b) Fresh PBMCs were either pretreated with MMC (50 μg/ml MMC for 45 minutes at 37°C) or untreated, stimulated with immobilized OKT-3 for 2 days, and then examined for OX40L expression on select lymphocyte subpopulations by FCM. (c) Fresh PBMCs were stimulated with immobilized OKT-3, 10 μg/ml phytohemaglutinin A, 25 ng/ml PMA, or anti-CD3/anti-CD28-conjugated magnetic beads for 24 hours either in the presence or in the absence of 10 μg/ml MMC and then examined for OX40L and OX40 expression by FCM. (d) T cells that were previously activated with immobilized OKT-3 for 3 days were restimulated with immobilized OKT-3 in the presence or absence of MMC for 24 hours. OX40L and OX40 expression was examined by FCM. Representative data of three independent experiments using two different donors are illustrated.

### Effect of other DNA synthesis inhibitors, ultraviolet (UV), and stresses on OX40L induction

To determine whether OX40L induction was unique to MMC treatment of *in vitro*-activated T cells or a general attribute of inhibitors of DNA synthesis, a variety of other DNA-damaging methods such as X-ray irradiation and 5-FU treatment were tested. As illustrated in Figure 2a, both treatments induced OX40L on activated T cells in a dose-dependent manner. The optimum doses of MMC, 5-FU, and x-ray for the maximum induction of OX40L on activated T cells were 6.3 to 12.5 $\mu$g/ml, 100 $\mu$g/ml, and 8-16 Gy, respectively. Treatment of PBMCs with optimal levels of 5-FU and MMC in combination followed by *in vitro* activation with anti-CD3 slightly enhanced the level of OX40L expression by T cells but the cell viability was reduced, possibly due to increased cytotoxicity (data not shown).

In an attempt to explore other conditions that might induce OX40L expression by T cells, we tested the exposure of aliquots of PBMCs to the DNA-damaging UV irradiation and exposure to heat and oxidative shock. Preliminary results of these studies indicated that an exposure of PBMCs to either UV-A or UV-B for a long period was very cytotoxic because most cells died by 24 hours following exposure (data not shown). However, exposure to sublethal doses of UV-B, but not UV-A, followed by short-term culture in the presence of immobilized anti-CD3 for 18 hours demonstrated a moderate increase of OX40L$^+$ cells above that seen with medium treatment (Figure 2b). In addition, neither exposure to heat shock nor oxidative stress by exposure of PBMCs to $H_2O_2$ had any detectable effect on the induction of OX40L expression following anti-CD3 activation (Figure 2c). These data highlight the effect of DNA stress on the induction of OX40L following *in vitro* activation of T cells.

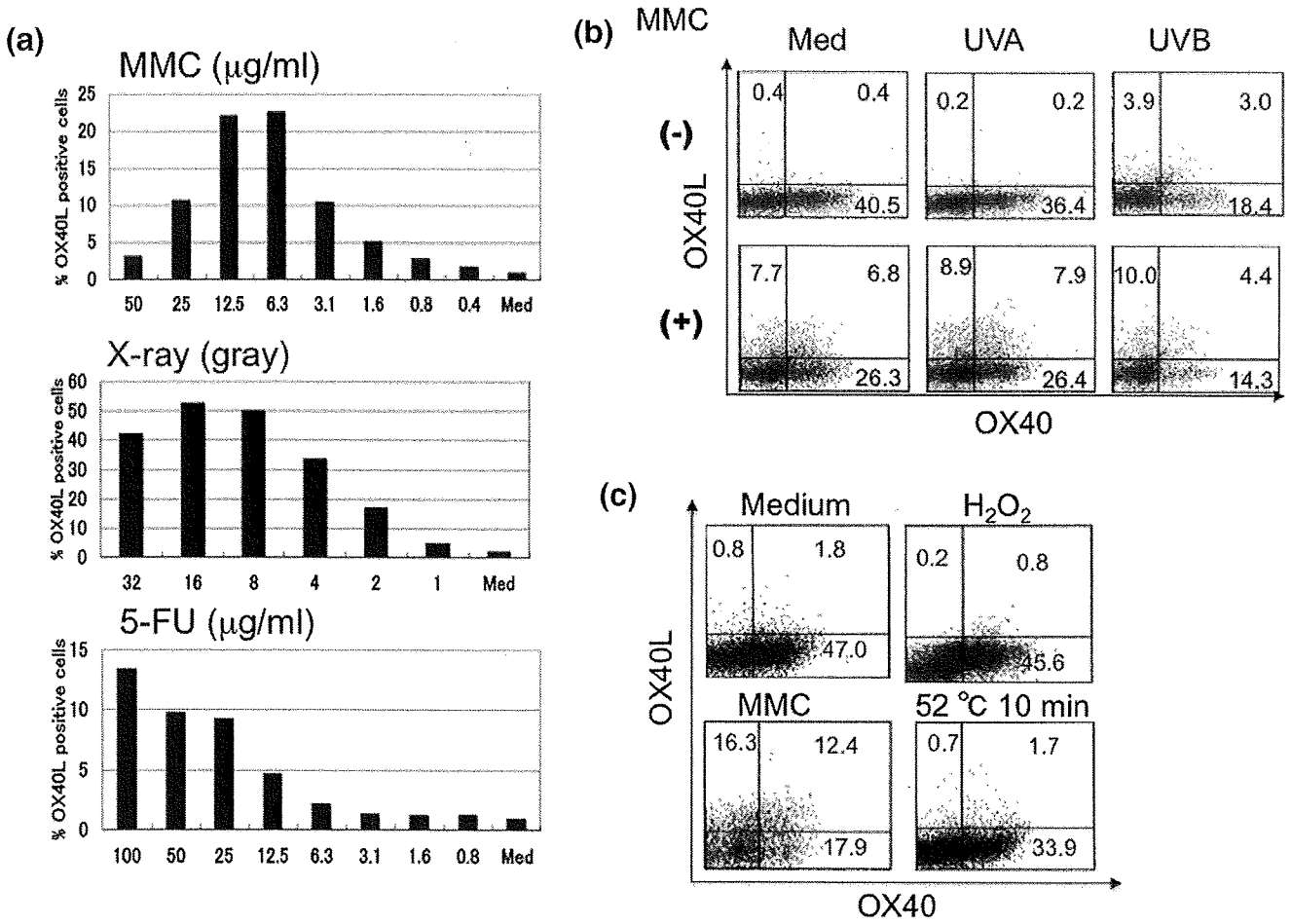


**Figure 2.** Dose response of OX40L induction on activated lymphocytes by exposure to DNA-damaging drugs and X-ray irradiation and the effect of UV irradiation, oxidation, or heat stress. (a) Fresh PBMCs were either untreated or pretreated by exposure to various doses of x-ray and stimulated with immobilized OKT-3 either in the presence or in the absence of grated concentrations of MMC or 5-FU for 24 hours. The frequency (%) of OX40L-positive cells was determined by FCM. (b) PBMCs were irradiated with sublethal doses of UV (UV-A at 365 nm for 81 seconds or UV-B at 254 nm or 60 seconds at 10 $\mu W/cm_2$) and then stimulated with immobilized OKT-3 for 18 hours in the presence or absence of MMC (10 $\mu$g/ml). Then, live lymphocytes were examined for the expression of OX40L and OX40 using standard FCM. (c) PBMCs were either untreated or preheated for 10 minutes at 52°C and then stimulated with immobilized OKT-3 for 24 hours in the presence or absence of 12.5 $\mu$g/ml $H_2O_2$ or 10 $\mu$g/ml MMC. The viable lymphocytes were then examined for OX40L and OX40 expression by FCM. Representative data of five independent experiments using three different donors are illustrated.

## Effect of inhibitors of RNA and protein synthesis and T-cell activation on OX40L induction

We next tested the effects of inhibitors of RNA and protein synthesis on OX40L induction following anti-CD3 activation. As illustrated in Figure 3, neither Act-D nor CHX induced OX40L expression by activated T cells. Of interest was the finding that these two drugs not only inhibited the MMC-induced OX40L expression by T cells, but also inhibited OX40 expression. Thus, it is clear that new RNA and protein syntheses were required for the induction of not only OX40L but also OX40 by activated T cells. In addition, CsA, which is known to block T-cell activation at an early activation step, also interfered with both OX40L and OX40 induction, supporting the view that cell activation was an important requirement for OX40L expression by activated T cells.

## Time course of OX40L expression and OX40L localization

Time-course experiments were performed to study the kinetics of OX40L induction. Fresh PBMCs were cultured in anti-CD3 mAb-coated plates in the presence of MMC for 1 to 72 hours and then examined for OX40L expression. As summarized in Figure 4a, the expression of OX40L became apparent as early as 1 hour after activation, and the percentage of positive cells gradually increased over time up to 72 hours. The decrease in cell viability following 72 hours in culture limited our ability to examine the induction of OX40L beyond this time period.

It was reasoned that one explanation for our failure to detect OX40L by non-MMC-treated *in vitro* anti-CD3 activated T cells could be due to the potential shedding of this molecule into the culture medium. We thus quantitated the levels of soluble OX40L in the culture supernatants and cell lysates of non-MMC-treated anti-CD3 activated cells using our in-house-developed OX40L and OX40 sandwich ELISA kits. As illustrated in Figure 4b, whereas OX40L was readily detected in the control MMC-treated activated cell lysates, there was no detectable level of OX40L in the culture supernatants of the MMC-untreated activated PBMCs. In addition, the level of cell-associated OX40L in the MMC-untreated activated PBMC was significantly lower than that of MMC-treated activated PBMCs. Of interest, the levels of OX40 in the cell lysates demonstrated an opposite trend with higher relative levels in MMC untreated compared with MMC-treated anti-CD3 activated cells. These data demonstrate that our failure to detect OX40L on non-MMC-treated *in vitro* anti-CD3-activated cells was not secondary to the shedding of this molecule. An alternative explanation could be that our failure to detect OX40L is due to homotypic binding of the OX40 to its cognate ligand OX40L in a manner that prevents the binding of the mAb being utilized for flow analysis. To address this issue, we treated PBMCs with a blocking anti-OX40 mAb (clone W4-54) during cultivation. The addition of such a blocking antibody still failed to demonstrate any detectable increase in the levels of OX40L on the cells following anti-CD3 activation and, furthermore, did not lead to any detectable levels of soluble OX40L in the culture supernatants (data not shown). These data further support the idea that both inhibition of DNA synthesis and activation are required for the induction of OX40L expression by activated T cells.

## OX40L induced on T cells is functional

To examine whether OX40L molecules expressed by the MMC-treated activated human T cells were functional, we tested the ability of these cells to bind soluble biotinylated OX40 along with OX40L. Figure 5 (top) illustrates that MMC-treated activated T cells clearly bind soluble OX40 and at much higher levels than that of control MMC-untreated activated T cells. To rule out a role for the FcR because the soluble OX40 utilized was a fusion protein with Fc portion of the mouse IgG2a, sample cells were preincubated with purified mouse IgG2a at 100 $\mu$g/ml and then analyzed for sOX40 binding. The blocking of FcR failed to influence the binding profile of sOX40, providing suggestive evidence that the binding of sOX40 was not likely due to FcR involvement (data not shown). In addition, the blocking of potential homotypic OX40-OX40L interaction by the addition of a blocking anti-OX40 mAb resulted in enhanced binding of sOX40 by both

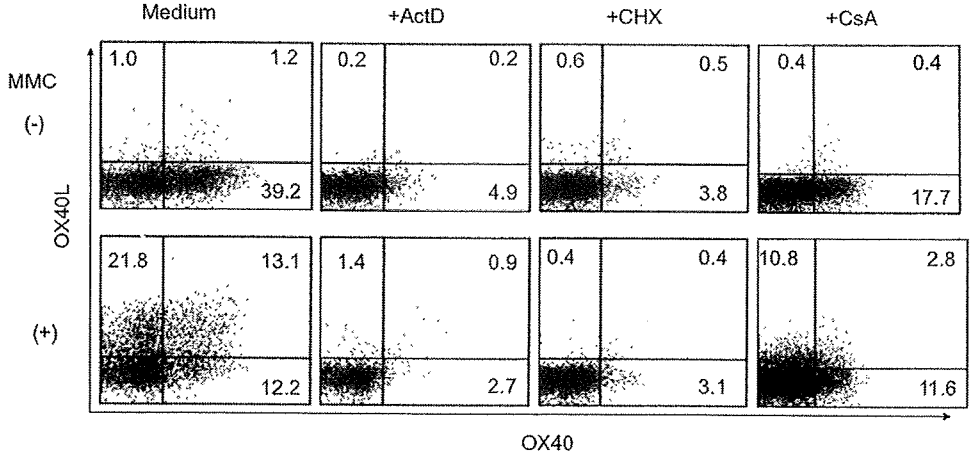


**Figure 3.** Requirements of RNA and protein syntheses for OX40L induction. Fresh PBMCs were stimulated with immobilized OKT-3 in the presence or absence of 10 $\mu$g/ml MMC and/or 1 $\mu$g/ml Act-D, 10 $\mu$g/ml CHX, or $5.5 \times 10^{-7}$ M CsA for 24 hours and then examined for OX40L expression by FCM. Representative data of five independent experiments using three different donors are illustrated.

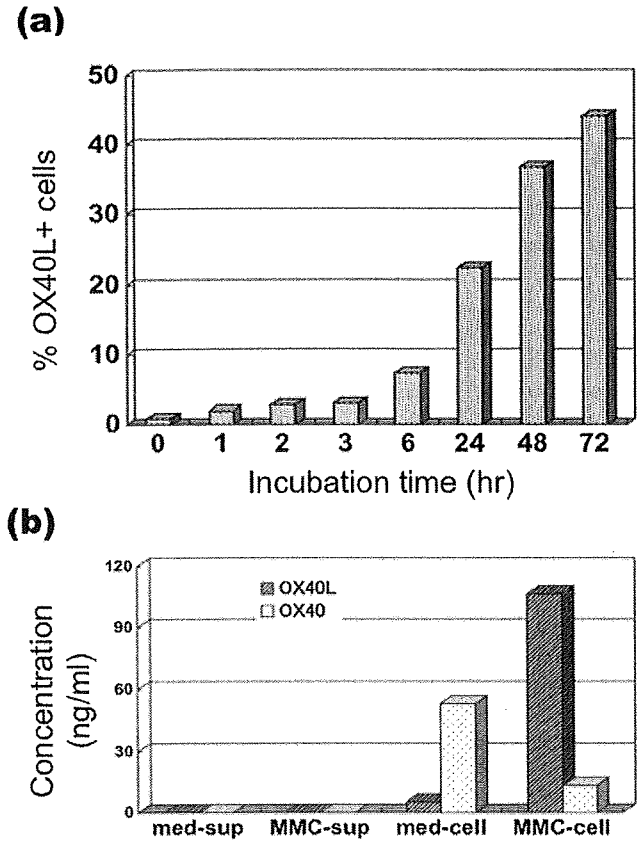


**Figure 4.** Time course of OX40L induction and its localization. (a) Fresh PBMCs were activated with immobilized OKT-3 in the presence of 10 $\mu$g/ml MMC for various periods of time. At each time point, the frequency of viable OX40L$^+$ lymphocytes within the lymphocyte gate was analyzed by FCM. (b) Fresh PBMCs were activated with immobilized OKT-3 either in the presence of 10 $\mu$g/ml MMC or in medium for 24 hours, and then culture supernatants (-sup) and cell lysates ($1 \times 10^6$ cells/ml) (-cell) were examined for concentrations of OX40L and OX40 using our in-house ELISA kits. Representative data of five independent experiments using three different donors are illustrated.

MMC-treated and untreated T cells (data not shown), indicating that a certain level of homotypic OX40-OX40L interaction does occur at the cell surface. Thus, these data suggest that OX40L molecules on the T cells were indeed functional, at least as determined by their ability to bind to their cognate receptor. On the contrary, similar studies conducted on analyzing the binding of sOX40L demonstrated that MMC-treated activated T cells displayed relatively lower levels of binding of sOX40L compared with MMC-untreated controls, indicating that a balance must exist in the expression of OX40L and OX40 being synthesized by T cells depending on the conditions of T-cell activation.

### Induction or enhancement of OX40L, CD27L, and CD30L expression in the MMC-treated activated T cells *in vitro* and *in vivo*

In efforts to determine whether exposure to a DNA stress-inducing agent uniquely influenced OX40L expression or whether such exposure generally influences the expression of other TNFSF of cell surface molecules following *in vitro* activation, we also examined the expression of CD27L, CD30L, FasL, TRAIL, and TNF-$\alpha$ in addition to a variety of other cell surface molecules. Results of these studies demonstrated that the MMC treatment following anti-CD3 activation led to significant increases in the expression of CD27L and CD30L on T cells, but the expression levels of the other three TNFSF molecules known as death-receptor ligands, FasL and TRAIL and TNF-$\alpha$, were not significantly different under these stimulation conditions.

Finally, in efforts to determine whether such induction of OX40L on T cells by MMC treatment and activation also occurred *in vivo*, we utilized our humanized mouse model. Human T cells are immediately activated following transfer into a xenogeneic mouse [23]. Thus, we did not use any exogenous stimulating agents in these experiments. Fresh human PBMCs were transplanted i.p. into immunodeficient mice followed by MMC injection. After 24 hours, these mice were sacrificed and cells from the spleen and peritoneal cavity were collected and then examined for the expression of OX40L together with CD27L and CD30L. As illustrated in Figure 6b, HLA class I-gated live human lymphocytes recovered from the MMC-treated mice expressed high levels of OX40L, as well as CD27L and CD30L, in contrast to MMC-untreated controls. These results indicate that induction or enhanced expression of OX40L, CD27L, and CD30L by human T cells indeed occurred *in vivo* by exposure to DNA-damaging agents and cell activation.

## Discussion

One of the objectives of the present study was to address the original question as to whether cell proliferation was

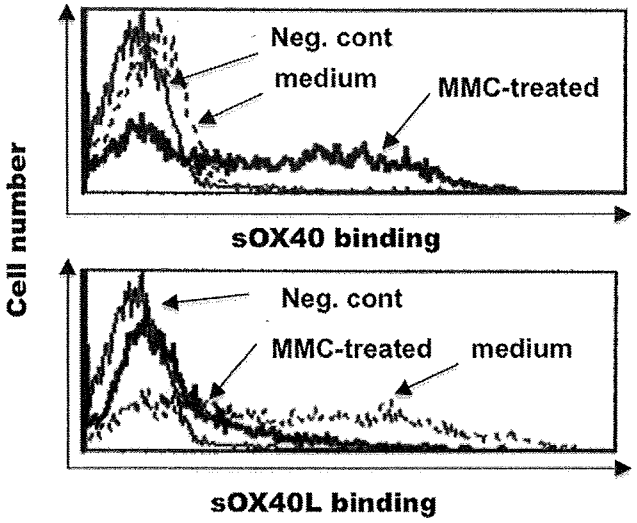


**Figure 5.** The OX40-binding capacity of the OX40L induced on MMC-treated activated T cells. Fresh PBMCs were activated with immobilized OKT-3 either in the presence or in the absence of 10 $\mu$g/ml MMC for 24 hours. Cell samples were washed, preincubated with Fc-blocking buffer, and then stained with biotinylated soluble OX40 or OX40L followed by streptavidin-PE staining and FCM analysis. Representative data of five independent experiments using three different donors are illustrated.

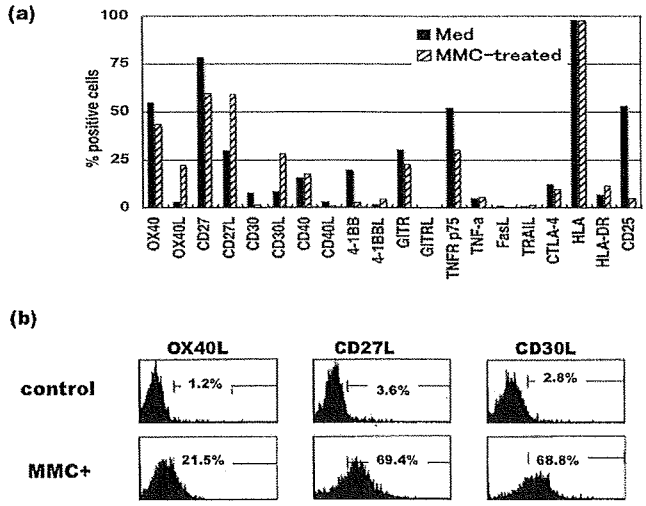


**Figure 6.** Enhanced expression of the TNFSF molecules CD30L and CD27L, together with OX40L on MMC-treated activated T cells both *in vitro* and *in vivo*. (a) Fresh PBMCs were activated with immobilized OKT-3 either in the presence of 10 $\mu$g/ml MMC or in medium for 24 hours, and then the viable lymphoid cells were analyzed for cell surface phenotype using a variety of mAbs. The percentage of positive cells is reported. Representative data of five independent experiments using at least three different donors are illustrated. (b) Immunodeficient mice (two animals per group) were engrafted with $1 \times 10^7$ fresh human PBMCs i.p. followed by immediate injection with 620 $\mu$g MMC or PBS (control). After 24 hours, these mice were sacrificed and their spleen cells and cells within the intraperitoneal cavity were harvested and pooled. The levels of cell surface expression of OX40L, CD27L, and CD30L on HLA class $I^+$ human lymphocytes were examined by FCM. Representative data of three independent experiments using two different donors are illustrated.

necessary for OX40L induction on activated T cells. Of interest is our finding that T-cell activation under DNA synthesis-inhibiting conditions rapidly induces the cell surface expression of OX40L, which is dependent on both RNA and protein syntheses *in vitro* and *in vivo*. The DNA damaging agents that induce OX40L expression include irradiation with x-ray and UV and anticancer drugs. Therefore, the phenomenon of OX40L induction on T cells may be not as rare an event in the normal life of humans.

The precise mechanism for the present observation is unknown at present. However, there are several potential explanations for the observed results. First, OX40L is synthesized as a result of a DNA repair process, in which $OX40L^+$ T cells may rescue $OX40^+$ T cells by stimulating an antiapoptotic pathway via OX40 signaling [8,24]. On the other hand, OX40L may function as a rescue molecule for such DNA-damaged activated T cells when stimulated with OX40. Second, high levels of OX40L on T cells may stimulate coexisting OX40-positive T cells to ameliorate emergency conditions induced by exposure to radiation and anti-DNA drugs via suppressing potent T helper 1 (Th1) conditions [13]. Third, OX40L expression may favor the clearance of DNA-damaged apoptotic cells by scavenger cells such as macrophage or dendritic cells. Although it is not known whether OX40L functions as an "eat-me" signal of apoptotic T cells [25], OX40L may facilitate the adhesion between apoptotic T cells and phagocytes such as DCs that are induced to express OX40 under certain conditions [26]. Because DCs are stimulated by exposure to apoptotic PBMCs activated via TCR [27], it is of interest to test whether OX40L on dying activated T cells is involved in the enhancement of antigen-presenting functions of DCs.

The potential benefits of OX40 stimulation by recombinant OX40L or agonistic antibody [28-30] on the therapy of some diseases, especially cancer, have been extensively investigated utilizing murine models [6,31,32]. One of the important roles of OX40 expression during immunotherapy is to maintain antigen-specific effector memory T cells [14,33,34]. In addition, results of some recent studies have revealed that OX40 triggering blocks regulatory T-cell function and thus facilitates T-cell-mediated tumor rejection [35,36]. These findings suggest that triggering of OX40 could have important therapeutic implications. In this regard, OX40L-expressing autologous T cells freshly prepared *in vitro* or *in vivo* may be good candidates that would be safe and have limited unnecessary side effects. Furthermore, because soluble recombinant OX40L molecules are less effective in activation than oligomers [29], cell-associated OX40L expressed on the cell surface may facilitate OX40 ligation more strongly than the soluble recombinant OX40L. Because MMC and irradiation have been generally used for the treatment of cancer in humans, simultaneous administration with humanized anti-CD3 antibody may induce a substantial number of OX40L-expressing T cells *in vivo*. Alternatively, such OX40L-positive T cells can be easily generated *in vitro* in large quantities for adoptive transfer studies by long-term cultivation of PBMCs in the presence of IL-2 and anti-CD3/anti-CD28 antibodies. Such therapeutic strategies must be clearly verified using our humanized mouse model.

Several agents that trigger OX40L expression in a variety of cell lineages have been previously reported, including thymic stromal lymphopoeitin, TNF-$\alpha$, lipopolysaccharide (LPS), or CD40 ligation for DCs [11,13,37], CD40 ligation and mitogens for B cells [10,38], IL-12 for murine T cells [14], CD16 or Ig-like receptor ligation for human NK cells [15], Fc-$\varepsilon$RI ligation for human mast cells, TL1A and death receptor 3 ligand for murine $CD4^+CD3^-$ accessory cells, and IL-4 and TGF-$\beta$ for human T cells [18]. On the other hand, down-regulating factors for OX40L expression have also been reported, including IL-12 for human T cells [18], type-I interferon for human mast cells [39], and IL-4 for murine T cells [14]. It remains to be established as to the mechanisms by which IL-12 and IL-4 function differently on OX40L induction between human and murine T cells. In addition, our preliminary study demonstrated no apparent induction of OX40L on murine splenocytes following x-ray irradiation and stimulation (G. Matsuzaki, K. Okuma and Y. Tanaka, unpublished data). Thus, there might be species-specific differences associated with OX40L induction or suppression by T cells and potentially also the biological outcomes of such OX40L-OX40 interactions. One example for the latter is that whereas mouse $CD4^+$ T cells acquire longevity following ligation of OX40 [14], human Th1 $CD4^+$ T cells have been shown to undergo apoptosis as a result of OX40 ligation [17]. A possible explanation for these discrepancies may be related to exposure to different environmental conditions and differences in the process of aging in the two species. Whereas mouse T cells are obtained from young mice (younger than a

few months) that have been housed in an specific pathogen free (SPF) environment, human T cells are obtained from adults having been exposed to irradiation, various microorganisms, and anti-DNA substances. Thus, it can be speculated that, as a result of aging in a natural environment (non-SPF environment), human immune systems are more frequently exposed to OX40L than the immune systems of naive mice. Because OX40L transgeneic mice suffer from immunological disorders such as autoimmune diseases [40], it is reasonable to assume that human T cells are less responsible for OX40L stimulation than murine T cells as a result of homeostasis maintenance.

Taking into consideration that DNA damage is a daily event in human life and one of the major contributors to the senescence of cells, it also seems possible that there could be a relationship between OX40L expression and senescence of T cells. Indeed, OX40L can be induced in T cells after long-term and repeated activation *in vitro* [18,41] without exposure to additional exogenous DNA-damaging agents. Furthermore, levels of soluble OX40L in serum samples are higher in aged humans [42] than in young adults. Thus, it will be interesting to explore both the relationship between telomere length and OX40L expression in T cells and the biologic meaning of OX40L expression for T-cell senescence and homeostasis.

Previously, Kim *et al.* [43] reported that 4-1BB (CD137), which is a member of the TNF receptor superfamily and normally induced on activated T cells as a costimulatory molecule, is rapidly induced on resting T cells by exposure to DNA-damaging agents to protect T cells from genotoxic stress. The major difference between 4-1BB and OX40L is that 4-1BB can be induced only by DNA damage without activation, whereas OX40L induction requires both signals. In addition, as illustrated in Figure 6, 4-1BB and its ligand expressing fresh lymphocytes were decreased by activation in the presence of MMC. Thus, the mechanism of and physiological role for OX40L induction by T cells are independent of 4-1BB activation although human OX40 and 4-1BB form a heterodimer in activated T cells and the heterodimer functions to suppress T-cell immune responses [44].

Further studies are in progress to determine the mechanisms by which DNA damage impacts activated T cells by expressing or downmodulating immunological molecules, including CD27L and CD30L, and their physiological roles in immunity. These studies may be relevant not only for the development of new immunotherapeutic strategies but also for our understanding of how DNA-damaged T cells influence the health of patients suffering from radiation exposure or receiving anticancer drugs.

## Acknowledgments

This work was supported by grants from a Grant-in-Aid for Scientific Research on Priority Areas from the Ministry of Education, Culture, Sports, Science, and Technology of Japan; Research on HIV/AIDS and Health Sciences focusing on Drug Innovation from the Ministry of Health, Labor and Welfare of Japan; and Japan Human Science Foundation.

## References

[1] Tanaka Y, Inoi T, Tozawa H, Yamamoto N, Hinuma Y. A glycoprotein antigen detected with new monoclonal antibodies on the surface of human lymphocytes infected with human T-cell leukemia virus type-I (HTLV-I). Int J Cancer 1985;36:549-55.

[2] Miura S, Ohtani K, Numata N, Niki M, Ohbo K, Ina Y, et al. Molecular cloning and characterization of a novel glycoprotein, gp34, that is specifically induced by the human T-cell leukemia virus type I transactivator p40tax. Mol Cell Biol 1991;11:1313-25.

[3] Godfrey WR, Fangoni FF, Harara MA, Buck D, Engelman EG. Identification of a human OX-40 ligand, a costimulator of CD4+ T cells with homology to tumor necrosis factor. J Exp Med 1994;180:757-62.

[4] Paterson DJ, Jefferies WA, Green JR, Brandon MR, Corthesy P, Puklavec M, et al. Antigens of activated rat T lymphocytes including a molecule of 50,000 Mr detected only on CD4 positive T blasts. Mol Immunol 1987;24:1281-90.

[5] Croft M. Costimulation of T cells by OX40, 4-1BB, and CD27. Cytokine Growth Factor Rev 2003;14:265-73.

[6] Sugamura K, Ishii N, Weinberg AD. Therapeutic targeting of the effector T-cell co-stimulatory molecule OX40. Nat Rev Immunol 2004;4:420-31.

[7] Watts TH. TNF/TNFR family members in costimulation of T cell responses. Annu Rev Immunol 2005;23:23-68.

[8] Song J, So T, Cheng M, Tang X, Croft M. Sustained survivin expression from OX40 costimulatory signals drives T cell clonal expansion. Immunity 2005;22:621-31.

[9] Compaan DM, Hymowitz SG. The crystal structure of the costimulatory OX40-OX40L complex. Structure 2006;14:1321-30.

[10] Stuber E, Neurath M, Calderhead D, Fell HP, Strober W. Cross-linking of OX40 ligand, a member of the TNF/NGF cytokine family, induces proliferation and differentiation in murine splenic B cells. Immunity 1995;2:507-21.

[11] Ohshima Y, Tanaka Y, Tozawa H, Takahashi Y, Maliszewski C, Deledpesse G. Expression and function of OX40 ligand on human dendritic cells. J Immunol 1997;159:3838-48.

[12] Imura A, Hori T, Imada K, Kawamata S, Tanaka Y, Imamura S, et al. OX40 expressed on fresh leukemic cells from adult T-cell leukemia patients mediates cell adhesion to vascular endothelial cells: implication for the possible involvement of OX40 in leukemic cell infiltration. Blood 1997;89:2951-8.

[13] Ito T, Wang YH, Duramad O, Hori T, Delespesse GJ, Watanabe N, et al. TSLP-activated dendritic cells induce an inflammatory T helper type 2 cell response through OX40 ligand. J Exp Med 2005;202:1213-23.

[14] Soroosh P, Ine S, Sugamura K, Ishii N. OX40-OX40 ligand interaction through T cell-T cell contact contributes to CD4 T cell longevity. J Immunol 2006;176:5975-87.

[15] Zingoni A, Sornasse T, Cocks BG, Tanaka Y, Santoni A, Lanier LL. Cross-talk between activated human NK cells and CD4+ T cells via OX40-OX40 ligand interactions. J Immunol 2004;173:3716-24.

[16] Kashiwakura J, Yokoi H, Saito H, Okayama Y. T cell proliferation by direct cross-talk between OX40 ligand on human mast cells and OX40 on human T cells: comparison of gene expression profiles between human tonsillar and lung-cultured mast cells. J Immunol 2004;173:5247-57.

[17] Takahashi Y, Tanaka R, Yamamoto N, Tanaka Y. Enhancement of OX40-induced apoptosis by TNF coactivation in OX40-expressing T cell lines in vitro leading to decreased targets for HIV type 1 production. AIDS Res Hum Retroviruses 2008;24:423-35.

[18] Kondo K, Okuma K, Tanaka R, Zhang LF, Kodama A, Takahashi Y, et al. Requirements for the functional expression of OX40 ligand on human activated CD4+ and CD8+ T cells. Hum Immunol 2007;68:563-71.